B and δ11B biogeochemical cycle in a beech forest developed on a calcareous soil: Pools, fluxes, and forcing parameters

P. Roux, D. Lemarchand, P.-O. Redon, M.-P. Turpault

B and $\delta^{11}B$ biogeochemical cycle in a beech forest developed on a calcareous soil: Pools, fluxes, and forcing parameters

P. ROUX*[1,2], D. LEMARCHAND[2], P-O. REDON[3] AND M-P. TURPAULT[1]

*corresponding author : philippe.roux@uliege.be

[1]BEF-INRAE, Centre Grans Est, Nancy, 54280 Champenoux, France

[2]Université de Strasbourg, CNRS, ENGEES, ITES UMR 7063, Strasbourg F-67084, France

[3]Andra, Centre de Meuse/Haute-Marne, 55290 Bure, France

Abstract

Rock weathering and biological cycling hold the development and sustainability of continental ecosystems, yet the interdependence of macro- and micro-nutrients biogeochemical cycles and their implications for ecosystem functioning remains unclear, despite being of particular importance in the context of global changes. This study focuses on the stocks, fluxes and processes constituting the biogeochemical cycle of boron. Vegetation, soils and solutions were monitored for a full year in a temperate beech forest developed on calcareous soil. Despite an overwhelmingly large B pool in soils, this study points to limited influence of weathering emphasizing the importance of vegetation cycling on this site. The biological imprint on the B cycle is marked by (1) a strong ^{11}B enrichment of solutions compared to the mineral source and (2) systematic correlations observed between B and other strongly recycled elements in all water samples. B isotopes are fractionated within the beech stand with higher values in leaves (23.5‰) and lower in fine roots (-11.7‰), suggesting that the light ^{10}B isotope is preferentially assimilated during plant growth. B isotopic data are consistent with a Rayleigh-like behaviour during xylem transfer leading to an ^{11}B enrichment in the higher parts of the trees, putting internal B transfer as the main driver of the large range of isotopic compositions between plant tissues. B apparent isotopic fractionations are observed in the annually produced biomass and total beech stand, albeit with different values: $\alpha_{xylem\text{-}biomass}$ = 0.980±0.009 and 0.990±0.002, respectively, suggesting ^{11}B transfer from old to new tissue. The developed model also points to an isotopic fractionation factor during B uptake much higher than previously evaluated ($0.979 < \alpha_{uptake} < 0.994$). Overall, this study demonstrates that B isotopes appear as a promising tracer of soil-plant interactions with particular emphasis on tree adaptation to B bioavailability in soil.

Keywords: boron isotopes, biogeochemical cycle, vegetation cycling, forest ecosystem, plant uptake,

1. Introduction

Chemical weathering and biological cycling are two major processes that control soil formation, nutrient release, and sustainability of continental ecosystems. Their study provides insights into the processes controlling the transfer of elements across ecosystem compartments and the balance between external nutrient supply (atmosphere and soil mineral weathering) and biological cycling, with consequences for ecosystem sustainability and their vulnerability to global changes. Among tracers used to investigate the transfer of matter in the critical zone, isotopes have been largely developed these last two decades (e.g. Fantle and DePaolo, 2004; Kimmig et al., 2018; Lemarchand et al., 2012; Opfergelt et al., 2017; Prunier et al., 2015; Schmitt et al., 2017; Schuessler et al., 2018; Spivak-Birndorf et al., 2018). B shares chemical properties with neighboring elements in the periodic table, Al, Si and C, which are major actors of mineralogical and biological reactions. This special position makes B and B isotopes interesting candidates to provide further understanding of physiological and bio-geochemical processes (e.g. Blevins and Lukaszewski, 1998; Gaillardet and Lemarchand, 2018).

B is a trace element with concentration in soil constituents varying from $mg.kg^{-1}$ level in quartz to tens of $g.kg^{-1}$ in some phyllosilicates and accessory minerals like tourmaline (Hu and Gao, 2008). B is considered to be a mobile element, similarly to K or Na, as shown by its long residence time in seawater (Lemarchand et al., 2000), but also shows enrichment in some secondary phases such as clay minerals or metal oxides compared to the continental crust (Goldberg, 1997). The large range of B isotopic compositions observed in soils and rivers is interpreted as the result of different weathering regimes and contributions of the vegetation cycling to B global cycle (Cividini et al. 2010; Ercolani et al. 2019; Lemarchand et al., 2012; Lemarchand and Gaillardet, 2006; Noireaux et al., 2021; Rose et al., 2000; Spivack et al., 1987; Schmitt et al. 2012; Williams et al., 2001).

In plants, B is an essential micronutrient involved in many fundamental physiological functions like sugar transport, nitrate assimilation or mycorrhizas development, but it is mostly known for its cell wall stabilization properties (Blevins and Lukaszewski, 1998; Brown et al., 2002;

O'Neill et al., 2001). Its restricted range between deficiency and toxicity makes B the second most widespread micronutrient worth considering after zinc and requires particular care in many agricultural systems (Shorrocks, 1997). Plants therefore require a continuous supply of sufficient B , but also control over internal B distribution to sustain optimal growth (Reid, 2014). Briefly, B is primarily passively absorbed by plant roots as uncharged boric acid from soil solutions, with active absorption only mentioned under B-limiting conditions (Hu and Brown, 1997). Once absorbed, B follows the transpiration stream (xylem) to the leaves where it is partitioned between soluble compounds and cell walls (Reid, 2014). During uptake and transfer, diffusional gradient between the xylem and the surrounding tissue allows passive unloading of B. This process can be facilitated by boron specific transporters or channels whose activation depends on B availability in soil solutions (Miwa and Fujiwara, 2010; Shao et al., 2021; Tanaka et al., 2008; Takano et al., 2002, 2006, 2010; Yoshinari and Takano, 2017). The translocation of B towards the different plant organs after sugar synthesis remains poorly understood as it is mostly depending on the existence of suitable, plant-specific, complexing molecules (Gupta, 1993; Reid, 2014).

B concentrations vary in plants from a few $mg.kg^{-1}$ to hundreds of $mg.kg^{-1}$ with large variations between organs, plant species and soil content (Ozturk et al., 2010). However, most studies focused on either crop plants or leaves, which makes the partitioning and overall B stock difficult to assess at the ecosystem scale. First attempts to measure B isotopes in different plant organs were made through ^{10}B labeling experiments to assess the transfer mechanisms of B (Marentes et al., 1997; Vanderpool and Johnson, 1992). To date, authors have determined B isotopic compositions in plants mostly in the context of food authentication, and the published values span a large range of values, from -25‰ to +40‰, with most of the variability being related to that of the local bedrock (Roux et al., 2015; Serra et al., 2005; Vogl et al., 2011; Wieser et al., 2001). To our knowledge, few studies have focused on intra-plant B isotope variations despite their potential insight in plant metabolism, crucial to fully understand the role of B in ecosystem functioning. Recently, a study by Sun et al. (2018) shown strong variations between structural and soluble B

within deciduous shrub species and observed a preferential accumulation of ^{11}B within the structural part. Geilert et al. (2019), on the other hand, have shown a vertical stratification of $\delta^{11}B$ data along the xylem path with low values in roots and high values in leaves. This is suspected to result from a preferential loading of ^{11}B to growing meristems facilitated by B transporters. Nevertheless, whether B transport network or its partitioning between soluble and structural compounds controls $\delta^{11}B$ remains an open question.

So far, only few studies attempted to establish the B biogeochemical cycle. Park and Schlesinger, (2002) as well as Schlesinger and Vengosh, (2016) determined the global B fluxes using previously published data but did not provide values for biological cycling. Cividini et al. (2010) monitored the fluxes of B and B isotopes in the Strengbach forest watershed (Vosges mountains, France) and showed a strong biological cycling of this element, up to 5 times higher than the B flux from bedrock weathering whereas this ratio rises up to 11 in the Mule Hole forest watershed in India (Gaillardet and Lemarchand, 2018). However, the mechanisms explaining the differences in terms of isotopic compositions between vegetation and bulk soil in both studies remain unclear. Chetelat et al, (2021) have recently modelled B isotopes in forest ecosystems and shown a transient enrichment in ^{11}B in biomass relative to that of steady-state caused by plant growth. Nevertheless, this model remains unconstrained through lack of available data. Finally, recent studies showed rapid B release during litter decomposition in case of no B deficiency, indicating that B is chemically complexed to water soluble molecules in leaves, whereas it is mostly bounded to cell walls in B deficiency conditions (Kot *et al.*, 2016; Lehto *et al.*, 2010a, b)

Based on a full year of comprehensive monitoring, this study aims at establishing detailed pools and fluxes of B and B isotopes within a forest water-soil-plant system developed under temperate climate. Their relationships with macro-nutrients and environmental forcing parameters are then discussed.

2. Materials and methods

2.1. Study site

This study was conducted at the beech forest experimental site located in Montiers-Sur-Saulx, Northeastern France (Meuse, France, 48°31'55" N / 5°16'8" E). This experimental site is part of the AnaEE network (Analysis and Experimentations on Ecosystems, https://www.anaee-france.fr/). This site has been co-managed since 2012 by the French National Research Institute for Agriculture, Food and Environment (INRAE-BEF) and by the French National Agency for Radioactive Waste Management (Andra) in the framework of its long-term environmental observatory (OPE). The Montiers site covers two soil sequences of a total of 143 ha (70 ha and 73 ha) in the forested area at an altitude ranging from 319 m to 400 m. The local climate is characterized as semi-continental with an annual temperature of 12.6°C with monthly averages ranging from 4.4 to 21.6°C and an average precipitation rate of approximately 1100 mm.

The vegetation of Montiers is mainly composed of an even-aged beech (≈ 60 years; 88% of total stems), but other species such as maple (6.1%), whitebeam (1.7 %), Ash tree (1.3 %), oak (1.2%), Hornbeam (1.0%) and wild cherry (0.4%) are also present. The humus can vary on the site from mull to acid-mull.

The geology of the Montiers study site consists in two geological layers: an underlying Jurassic (Tithonian) limestone covered by lower Cretaceous (Valanginian) acidic detrital sediments. The calcareous bedrock contains up to 3.4% of clay making the regolith a clay rich soil layer due to bedrock decarbonation. The detrital sediments are a combination of clay, silt, coarse sand and iron oxides that result from multiple deposition events. Due to the differences in thickness of the sediment layer, the soil type displays an acidic gradient with a *Dystric Cambisol* at the top of the hillslope, an *Eutric Cambisol* and a *Rendzic Leptosol* on the lower parts of the soil sequence. A schematic representation of the soil profiles as well as the main characteristics of these different soil types can be found in Calvaruso et al. (2017) and Kirchen et al. (2017). In this study, we focused on the calcareous soil (*Rendzic Leptosol*). It is only 30cm deep with a textural distribution strongly

126 enriched in clay (up to 50%). The Jurassic limestone bedrock can be found all along the soil profile
127 with a rock volume varying from 2.3% at the surface to 36.4% at 30cm. Neither pH nor CEC
128 parameters vary strongly with values averaging 6.9 and 22.7 cmol.kg^{-1}. The soil is covered by an
129 eutrophic mull humus. More detailed information can be found in Turpault et al. (2018).

130 ***2.2. Instrumentation and sampling***

131 The *Dystric Cambisol*, *Eutric Cambisol* and *Rendzic Leptosol* have been instrumented since the
132 end of 2011 to allow the monitoring of the stocks and fluxes of nutrients in soil, vegetation, water,
133 dust, and litter. Each type of soil covers an area of about 1 ha and is divided in four equal replicates
134 of 2500 m^2. Out of the replicates, three are instrumented while one is left intact for future
135 experimentations.

136 ***2.2.1. Soil***

137 The soil and subsoil samples were collected in March 2011 down to a maximum depth of 35
138 cm. The soil profile was divided in layers of varying thickness from 5 cm to 15 cm. After drying at
139 35°C, soil samples were weighed and sieved at 2 mm to obtain the fine earth (<2 mm). About 10g of
140 the fine earth fraction were ground and sieved at 50 µm.

141 ***2.2.2. Humus***

142 Humus samples have been collected in June 2010 using a calibrated metal frame of 0.1 m². The
143 samples were dried in a ventilated oven at 65°C until complete dryness. Dried samples were then
144 merged per substation and sieved to obtain a homogeneous average sample. A sub-sample was
145 ground in a ring roller mill before storage at room temperature.

146 ***2.2.3. Beech stand***

147 *Aboveground plant biomass*: In winter 2009, during the establishment of the study site, a
148 total of 25 trees along the soil sequence were cut down to homogenize stand characteristics,

149 evaluate biomass and establish allometric equations. Additional sampling details can be found in
150 Calvaruso et al. (2017). 4 trees grown on the *Rendzic Leptosol* were selected for B measurement.
151 The trees were divided in several parts that were weighted on site. The trunk was separated into
152 bark and wood samples while the branches were separated into different diameter classes according
153 to Henry et al. (2011). The selected samples for the characterization of aboveground plant biomass in
154 this study are: stem wood; stem bark; coarse branches wood (diameter > 7 cm); coarse branches
155 bark; medium branches wood and bark (4 < diameter < 7 cm) and fine branches wood and bark
156 (diameter < 4 cm). This separation is essential because of significant differences in the elemental
157 concentrations, density, and water content.

158 *Roots:* Fine roots were collected in March 2011 in the trenches dedicated for the
159 establishment of the soil profiles. In each horizon (0-5 cm, 5-15 cm), 100 g of soil containing roots
160 was collected from 3 sampling points. The separation of roots and soil were performed by shaking.
161 The roots were then immersed in milli-Q water and placed in an ultrasound bath for 15 min. This last
162 step was repeated until no soil particles were remaining onto the root after verification by binocular
163 microscope.

164 *Litterfall:* Litter samples were continuously collected for 12 weeks periods in 2012 except in
165 autumn when they were sampled every 8 weeks. Each litter sample integrates an entire season:
166 21/12/11-13/03/12 for winter, 13/03/12 – 05/06/12 for spring, 05/06/12 - 28/08/12 for summer,
167 28/08/12 – 23/10/12 for the summer-autumn transition and 23/10/12 – 17/12/12 for the second
168 part of autumn. The samples collected in October and December were merged to constitute an
169 average autumn sample. Litters were collected in 0.33 m^2 litterbags and were divided in three parts:
170 leaves (LL), wood (LW) and others (LO), and stored in paper bags at ambient temperature.

171 *Fresh leaves:* Fresh leaves were sampled on the 28/08/12 by shooting and weighed on site.
172 All vegetation samples were subsequently placed in an oven at 65°C until complete dryness. Dried

samples were then ground by a ring roller mill and dried again for two days before storage at room temperature.

2.2.4. Water compartments

The Montiers experimental site is equipped to allow water sampling from throughfalls to deep soil solutions. Water samples were collected in tanks that were sampled and emptied every 4 weeks between January and December 2012. In this study, we focused on 4 chosen timeframes: 17/01/12 - 14/02/12 for winter, 10/04/12 - 09/05/12 for spring, 03/07/12 - 31/07/12 for summer and 24/09/12 - 22/10/12 for autumn. Each period is thereafter respectively labeled Win, Spr, Sum and Aut. The lack of deep soil solutions for the summer samples imposed an additional sampling period between 31/07/12 – 28/08/12, hereafter labeled as Sum2. The selected hydrological compartments are:

Throughfalls (TF): Throughfalls were collected by four 0.38 m² polyethylene gutters (12 per station) placed under forest cover, radially to the stems, at 1.2 m above ground and connected to a 120 L polyethylene barrel placed in a pit belowground. The throughfalls collected by the gutters were then gathered per replicates on site. In this study, 3 replicates were analyzed for boron content and isotopic composition for each selected timeframe.

Stemflow (SF) were collected by polyethylene foam wrapped around the stem and connected to a 120 L, 150 L or 310 L recovery barrel, depending on the size of the tree. 6 collectors were set up in each substation (18 per station) and distributed among different stem circumferences. During the winter months (from November to March), only 2 collectors were functioning per replicate and the recovery barrels were placed underground to avoid water freezing. Before filtration in the laboratory, the beech stemflows of each substation were mixed to obtain one representative average sample.

196 *Gravitational water (soil solutions, GW):* soil solutions were sampled by 3 polyethylene
197 lysimeter plates at 0 cm, -10 cm and -30 cm depth. The lysimeter plates are connected to a 20 L
198 polyethylene bottle placed below ground.

199 During each sampling period, 250 mL of water was sampled from each collector and stored in
200 pre-cleaned high-density polyethylene bottles. Within 24 h, the samples were filtered in the lab using
201 0.45 µm acetate filters (47 mm diameter) and stored in a cold-room at 4°C in pre-cleaned high-
202 density polyethylene bottles before major elements and boron analyses.

203 ### *2.3. Analytical procedure*

204 #### *2.3.1. Reagents*

205 Ultra-pure water (18.2 MΩ.cm^{-1}) was provided by a Milli-Q Gradient water purification
206 system (Millipore, Billerica, MA,USA). The HCl and HNO_3 acids used in this study were sub-boiled in a
207 Teflon DST-1000 Savillex (Eden Prairie, MN, USA) distillation system. The alkali fusion was performed
208 using Pt-Au crucible and powdered analytical grade K_2CO_3. The sample purification steps were
209 performed in a clean room (class filter h14, class 1000) under a laminar flow box (filter class h15,
210 class 100) using two types of resin: the cation-specific BioRad AG50W-X12 and the boron specific
211 Amberlite IRA 743.

212 #### *2.3.2. Major elements concentration*

213 *Water and vegetation samples:* Concentrations of major cations in water (Al, Ca, Fe, K, Mg,
214 Mn, Na, P, S, Si) and vegetation samples (Al, Ca, K, Mg, Mn, Na, P, S) were measured by ICP-OES
215 (Agilent Technologies™ 700 series) at the BEF laboratory (INRAE Grand Est, Nancy) after microwave
216 acid digestion for vegetation samples (see §2.3.3 for details). Major anions were measured by Ion
217 Chromatography Dionex™ ICS-2100. TOC, TC, IC, and TN parameters were also determined in water
218 samples by TOC-L Shimadzu™. The analytical uncertainty is 10% (±2SD).

Soil and humus samples: Major elements expressed as oxides as well as trace elements were measured at the SARM laboratory (CNRS, Vandoeuvre-lès-Nancy, France, http://helium.crpg.cnrs-nancy.fr/SARM/) after lithium-borate alkali fusion by Thermo-Fisher ICap 6500 ICP-OES.

2.3.3. Boron extraction and purification

Vegetation samples: Boron from vegetation and litter was extracted by microwave acid digestion as described in Roux et al. (2015). Briefly, 100 mg of plant material were digested for 90 min at 800 W (≈ 5000 kPa; 250°C) using 10 mL of 1 N HCl-HNO_3 (1/3 – 2/3). The recovered solution was centrifuged at 4000 rpm for 20 min before being processed through a double purification procedure. The first step allowed the removal of most of the cations by ion chromatography using the resin BioRad AG50W-X12. Since silicon and DOC are not retained by this resin, a final micro-sublimation step was added to achieve satisfying level of purification.

Soil, humus and water samples: Boron from soil and humus samples was extracted by K_2CO_3 alkali fusion (40 min at 950°C – 50 mg of sample – 250 mg of K_2CO_3) and dissolved in 0.2 N HCl before being processed through a double purification procedure adapted from Lemarchand et al. (2012). The first step aimed at removing most of the major cation using 1.5 mL of cation exchange Bio-Rad AG50W-X12 resin (100–200 mesh) while the second step is aimed at extracting boron using 0.5 mL of the boron-specific Amberlite IRA 743 resin. Boron extraction from water samples was performed only using the boron specific Amberlite IRA 743 resin. Typically, 500 ng of boron were processed through the resin to keep the relative contribution of the procedural contamination as low as possible (≈ 12 ng, mainly coming from the alkali fusion step)

2.3.4. Boron concentration and isotope

Boron concentration measurements were performed on a quadrupole mass spectrometer at the Laboratoire d'Hydrologie et de Géochimie de Strasbourg (LHyGeS, University of Strasbourg) by

Isotopic Dilution (ID-ICPMS) following the procedure described in Roux et al. (2015) with a precision of 1% (2SD).

Boron isotopic compositions were determined at LHyGeS by a Finnigan-Neptune MC-ICPMS (Thermo Scientific, Waltham, MA, USA) using three different reference materials for control: JB2 ($\delta^{11}B$ = 7.74 ± 0.51‰, 2σ, n = 3 Geological Survey of Japan, Tokyo, Japan) as rock standards, NIST SRM 1570a ($\delta^{11}B$ = 25.74 ± 0.21‰, 2σ, n = 5, National Institute of Standards and Technology, Gaithersburg, MD 20899, USA) for plant material standard and ERM-AE120 ($\delta^{11}B$ = -20.08 ± 0.28‰, 2σ, n = 12, BAM Federal Institute for Materials and Testing, Berlin, Germany) as water standard. The B reference material NIST SRM 951 ($^{11}B/^{10}B$ = 4.0437, National Institute of Standards and Technology, Gaithersburg, MD 20899, USA) was used for correction of the instrumental mass bias occurring during $^{11}B/^{10}B$ measurements. Results are expressed in $\delta^{11}B$ (‰) values corresponding to the relative deviation from the NIST SRM 951 reference material expressed in permil (Eq. 1):

$$\delta^{11}B_{sample} = \left(\frac{\left({}^{11}B/{}^{10}B \right)_{sample}}{\left({}^{11}B/{}^{10}B \right)_{NIST\ SRM\ 951}} - 1 \right) \times 1000 \quad (1)$$

The analytical uncertainty for B isotope, based on repeated standards and duplicated samples, is 0.5‰ (2SD).

2.4. B pools and fluxes calculation

Surface normalized B pools and fluxes were obtained by multiplying the mass of solid or solution given in $kg.ha^{-1}$ by the B concentration in $g.kg^{-1}$. Pools are therefore expressed in $g.ha^{-1}$, monthly fluxes are expressed on a $\mu g.m^{-2}.d^{-1}$ basis and summed up to a yearly flux expressed in $g.ha^{-1}.y^{-1}$. Hereafter, we only detail fluxes and pools for which the calculation differs from the simple multiplication of B concentration by mass of solid/solution.

2.4.1. Soil

263 The B stock in the soil profile (in $g.ha^{-1}$) is calculated by summing the mass of each soil
264 horizon ($kg.ha^{-1}$) multiplied by its respective B concentration ($mg.kg^{-1}$). The mass of a soil layer is
265 determined by correcting the volume of soil from the rate of stone, bedrock and density as described
266 in Calvaruso et al. (2017).

267 ***2.4.2. Water samples***

268 To transform the water stemflow volumes measured on site into water fluxes, we used the
269 stem circumference at 130 cm (C130) as the main factor explaining the variability between
270 individuals. Multiple linear correlations between C130 values and stemflow volumes allow to
271 distinguish between C130 classes. The stemflow fluxes are then determined for each C130 class by
272 the equation found in Turpault et al. (2018).

273 Fluxes of dissolved B by soil drainage have been determined using the B concentrations
274 measured in pore waters of each soil layer and water fluxes calculated by the hydrological BILJOU©
275 model (Granier et al., 1999) and from calibrations determined by Kirchen et al. (2017).

276 Since waters from the different hydrological compartments were not collected continuously
277 all throughout 2012 (only 5 monthly samples for each compartment, see §2.2.4 for details), we
278 extrapolated the B concentrations and isotopic compositions of throughfall (TF), stemflow (SF) and
279 soil solutions (GW0, GW10 and GW30) to fill missing data. Based on strong correlations with B/Na
280 and $\delta^{11}B$ in all ecosystem solutions, the K/Na chemical ratio is used as a proxy. The significance of
281 these observed correlations will be discussed below. The uncertainties are calculated as the standard
282 deviation of the difference between the modelled and the measured values for each compartment,
283 when available. Annual fluxes in throughfalls, stemflows and soil solutions were determined using a
284 Monte Carlo simulation using observed variability.

285 ***2.4.3. Beech stand***

286 The biomass of each forest stand was estimated in 2009 and 2014 using an allometric model
287 based on tree height, diameter at 130 cm and age of trees (Saint-André et al., 2005). The model was
288 calibrated, and its robustness verified on site using biomass measurements realized on 24 beech
289 trees equally distributed on the *Dystric Cambisol* and on the *Rendzic Leptosol*. Allometric equations
290 were also developed to determine the height of the trees from C130 and diameter at breast height
291 was measured on a yearly basis, allowing the estimation of the yearly aboveground biomass
292 production (for details see Calvaruso et al. (2017)). The aboveground biomass production is
293 calculated as the difference between the biomass calculated in 2014 and 2009 and is considered
294 linear along this period to derive an annual aboveground biomass production. Since the different
295 tree compartments were only sampled in 2009 for this study, both B pools in perennial biomass and
296 B fluxes from biomass production were calculated using the B concentrations measured in the 2009
297 fallen trees.

298 *Fine root biomass* - The total biomass in fine roots is calculated in each soil layer by summing the
299 fine-root biomass collected in the different soil aliquots and then multiplied by their respective mass
300 ratio to total soil.

301 *Fine root decay flux* – The fine-root turnover rate depends on the fine-root biomass and annual
302 production. In this study, The B flux from fine roots decay to the soil nutrient pool is calculated by
303 multiplying the B stocks in fine roots by the fine root turnover rate: 1.11 y^{-1} as determined for *Fagus*
304 *sylvatica* in Europe by Brunner et al. (2013).

305 *Harvest and exploitation of residuals* – The French National Forestry Office carries out a thinning of
306 the aboveground biomass every 7 years, which consist of thinning approximately 35 x 10^3 $kg.ha^{-1}$ on
307 the *Rendzic Leptosol* (Turpault et al., 2018). However, only the stem (69.2% of the biomass) and
308 coarse branches (8.5%) are exported while the smaller compartments (i.e. medium and small
309 branches, 22.3%) are left on the forest floor. Details are available in Calvaruso et al. (2017) and
310 Turpault et al. (2018).

2.4.4. Mass and isotope budget in the soil-plant system

The comprehensive dataset provided in this study allows quantifying the major B fluxes and associated isotopic compositions in forest ecosystems. Calculations are made on yearly fluxes and uncertainties are determined by Monte Carlo simulation. The terms used in the different equations are reported in *Table 1.*

Table 1: Definitions for equations and system components

Interactions with the canopy - Interactions between canopy and atmosphere are considered as B transfers through leaching of atmospheric particles/aerosols/gases, leaf exudation and canopy uptake via stomatal absorption (Adriaenssens et al., 2012). So far, gaseous B exchanges between atmosphere and leaves have never been reported and are therefore not considered here. The B flux and isotopic composition originating from canopy interactions can be expressed as follows:

$$F_{CL} = F_{TF} + F_{SF} - F_{Aw} \quad (2)$$

$$R_{CL} \approx \frac{(F_{TF}R_{TF} + F_{SF}R_{SF} - F_{AW}R_{Aw})}{F_{CL}} \quad (3)$$

Humus layer - The humus layer integrates the fluxes coming from canopy leaching, atmospheric deposition, organic matter mineralization, vegetation uptake and weathering processes (Dincher et al., 2020). Since neither vegetation uptake (Kirchen et al., 2017) nor any significant weathering flux (Dincher et al., 2020) have been observed within the humus layer, the B flux by mineralization of the humus layer is reduced to the difference between B export to the top soil (at 0 cm) and B inputs from throughfalls and stemflow. Furthermore, no significant variations in stock of major element had been observed between 2010 and 2018 (Dincher et al., 2020). Therefore, we assume that the humus layer

is at steady state, therefore inducing no isotope fractionation during decomposition, which lead to the following mass balance equations:

$$F_{\text{hum\_min}} = F_{0cm} - (F_{TF} + F_{SF}) \quad (4)$$

$$R_{\text{hum\_min}} \approx \frac{F_{0cm}R_{0cm} - (F_{TF}R_{TF} + F_{SF}R_{SF})}{F_{\text{hum\_min}}} \quad (5)$$

Vegetation uptake - The B flux absorbed by the tree roots is assumed mostly occurring in the shallow soil layer as it corresponds to the maximum root density zone (0-30cm) and no significant amount of fine roots have been quantified below 30cm (Turpault et al., 2018). It is calculated by summing the net biomass production and the cycling flux:

$$F_{upt} = F_{growth} + F_{cycling} \quad (6)$$

with $$F_{cycling} = F_{CL} + F_{litterfall} + F_{fine\ root\ decay} \quad (7)$$

3. Results

All B pools, annual fluxes and isotopic compositions constituting the B biogeochemical are reported in *Table 2* and *Figure 1*.

Table 2: B stocks (g.ha^{-1}), yearly flux (g.ha^{-1}.y^{-1}) and isotopic compositions (‰) constituting the B biogeochemical cycle in the Montiers temperate forest ecosystem

Figure 1: Biogeochemical cycle of B and B isotopes in the Montiers temperate forest ecosystem.

3.1. Soil

B concentrations in the soil range between 42 mg.kg^{-1} and 83 mg.kg^{-1} (*Table 3*), which are high compared to the mean continental crust (≈ 10 mg.kg^{-1}), but within the 10-100 mg.kg^{-1} range of

typical soil minerals (Lemarchand et al., 2012). Along the soil profile, B concentrations increase with depth from 0 cm to 30 cm followed by a decrease in the deepest subsoil layers, which is interpreted as the dilution of the B-rich clay minerals and Fe-oxides by the B-poor limestone. Despite strong variations in B concentrations, $\delta^{11}B$ values are homogenous along the soil profile as they range from -6.1‰ to -7.1‰. These $\delta^{11}B$ values are consistent with previous published work on shales (Noireaux et al., 2021). The isotopic compositions and concentrations of the bulk B-rich soil layers are also consistent with on-site clay minerals (220 $mg.kg^{-1}$; -5.0‰). All soil horizons show higher B concentrations than the underlying calcareous bedrock by at least a factor 5 ($[B]_{limestone}$ = 8.2 $mg.kg^{-1}$, *Table 3*). The overall B stock within the profile was determined at 135 $kg.ha^{-1}$ and a B isotopic composition of -6.9‰. Because of the general nature of soils and the large B pool compared to the other compartment (*Table 2*), we don't expect the sampling date between soil the other fluxes sampling to induce significant changes in the overall B biogeochemical cycle.

Table 3: B concentration ($mg.kg^{-1}$) and isotopic composition (‰) of soil, soil constituents, humus, beech stand and litter samples collected in the Montiers forest ecosystem.

3.2. Humus

Compared to the rest of the soil profile the mull samples show significantly lower B concentration of 19 $mg.kg^{-1}$ (*Table 3*). The humus B isotopic composition (+6.7‰) is significantly different from those of the soil profile. In terms of B budget, much less B is present in the humus (0.17 $kg.ha^{-1}$) than in the soil minerals by more than two orders of magnitude.

3.3. Beech stand

B concentrations vary over one order of magnitude between plant compartments, from 2.4 $mg.kg^{-1}$ in the stem wood to 33.6 $mg.kg^{-1}$ in the stem bark (*Table 3*). The B concentration in leaves, 26 $mg.kg^{-1}$, is consistent with previous studies on beech and other deciduous species (Cividini et al., 2010; Kot et al., 2016; Rosner et al., 2011). The B concentration decreases from the small branches (10.9 - 12.2 $mg.kg^{-1}$) to the coarse ones (2.4 – 3.2 $mg.kg^{-1}$, *Fig. 2*). B concentrations in fine roots are

intermediate compared to the other plant compartments and tend to slightly decrease with depth from 12.2 mg.kg^{-1} at 0 - 5 cm to 9.2 mg.kg^{-1} at 5 - 15 cm. The isotopic compositions of the different tree compartments sampled in this study range from -11.7‰ for the deepest fine roots to 23.5‰ in the leaves, thus covering approximately 30% of recorded B natural isotopic variations (*Fig. 2* and *Table 3*). $\delta^{11}B$ values increase vertically from roots to shoots through stem and branches, but also radially from wood to bark.

Figure 2: Boron concentration (mg.kg^{-1}) and isotopic composition (‰) of the different compartments of the beech stand.

The calculated B pools in the different beech stand compartments are reported in *Supplementary material, Table A.1*. The overall B stock in the perennial part of forest stand (stem and branches) is calculated at 571 ± 119 g.ha^{-1} with a mean isotopic composition of 5.0 ± 2.0‰. About 61% of the total B stock is in the stem (349 ± 78 g.ha^{-1}) and 39% in the branches (222 ± 41 g.ha^{-1}) with the small branches reaching 28% (160 ± 24 g.ha^{-1}). Because the perennial biomass integrates 50 years of development, we don't expect the 3 year gap with the fluxes sampling to significantly impact the overall B biogeochemical cycle.

3.4. Vegetation uptake, perennial and annual growth

From Eq.6 and 7, we calculate a vegetation uptake of 276.1 g.ha^{-1}.y^{-1}. The yearly B uptake by perennial biomass growth is estimated at 32.6 g.ha^{-1}.y^{-1} integrated between 2009 and 2014 (*Supplementary material, Table A.1*), which splits into 59% to the stem (19.2 g.ha^{-1}.y^{-1}), 25% to the young and small branches (8.0 g.ha^{-1}.y^{-1}) and the remaining 16% to the coarse branches (5.7 g.ha^{-1}.y^{-1}). However, perennial biomass only represents 14% of the total B vegetation demand while foliage production involves 119.8 g.ha^{-1}.y^{-1} (53%) and fine roots accumulate 73.6 g.ha^{-1}.y^{-1} (33%) of B. The fine root decay flux to the soil is estimated at 81.6 g.ha.y^{-1} (*Table 2, Fig. 1*) with a turnover rate of 1.11 y^{-1} (Brunner *et al.*, 2013).

3.5. Exploitation exportation and residues

The latest cut in 2016 led to a total removal of 184.5 g of B among which, 115.4 g were exported while the remaining 69.2 g have been left on site. This leads to a yearly exportation flux of 16.5 $g.ha^{-1}.y^{-1}$ and an exploitation residues flux of 9.9 $g.ha^{-1}.y^{-1}$ of B with a respective isotopic composition of 3.0‰ and 8.4‰ (*Table 2*).

3.6. Litterfall

B concentrations and isotopic compositions of the different types of litter are reported in *Table 3.* B concentrations in leaf litter samples display little variation throughout the year from 15.3 $mg.kg^{-1}$ in spring to 18.8 $mg.kg^{-1}$ in autumn (LL, $\bar{x}$ = 16.8 ± 1.5 $mg.kg^{-1}$, 1SD, n = 4). The wood litter has B concentrations ranging from 11.9 to 22.4 $mg.kg^{-1}$ (LW, $\bar{x}$ = 16.6 ± 4.3 $mg.kg^{-1}$, 1SD, n = 4) with the highest value in summer. The other litter components (LO) range from 5.6 to 20.0 $mg.kg^{-1}$ (LO, $\bar{x}$ = 12.5 ± 5.9 $mg.kg^{-1}$, 1SD, n = 4) with the highest value during winter. The B isotopic compositions span a large range of values from -0.2 to 21.3‰ related to the type of litter with leaf litter showing the highest values (6.9 to 21.3‰) followed by the LO samples (1.4 to 11.9‰) and the wood litter (-0.2 to 6.9‰). B concentrations and isotopic compositions show slight but parallel seasonal evolutions in leaf litter with higher values in summer and autumn, lower in winter, and lowest in spring. For the other type of litter, we observe a decrease from 20.0 to 5.6 $mg.kg^{-1}$ of the B concentrations throughout the sampling period while the isotopic compositions continuously increase from 1.4 to 11.9‰. The corresponding B fluxes from the litterfall vary over two orders of magnitude with values ranging from 0.1 to 52.6 $\mu g.m^{-2}.d^{-1}$ (*Supplementary material, Table A.2)*. B fluxes follow the seasonal growth with a maximum in spring for the LO samples (bud scales) and in autumn for the LL samples (senescence). The overall B flux and isotopic composition from litter samples constantly increases from winter (2.1 $\mu g.m^{-2}.d^{-1}$, 2.5‰) to autumn (53.4 $\mu g.m^{-2}.d^{-1}$, 19.1‰) and amount to a total of 72.3 $g.ha^{-1}.y^{-1}$ with an integrated isotopic composition of 17.3‰ (*Table 2*).

3.7. Water samples

B concentrations in throughfalls range from 2.7 to 11.7 µg.kg^{-1} ($\bar{x}$ = 11.4 ± 8.3 µg.kg^{-1}, 1SD, n=9) and from 6.4 to 38.3 µg.kg^{-1} in stemflows (*Table 4*). The isotopic compositions in throughfalls show seasonal variations with the lowest values during spring and winter (18.8 to 25.5‰) and the highest during autumn (33.6 to 37.2‰). Stemflows follow the same evolution than that of throughfalls but in a narrower range with 26.7‰ in winter and 34.7‰ in autumn.

The soil solutions have similar range of B concentrations than stemflows and higher than throughfalls with values ranging from 7.4 to 28.5 µg.kg^{-1} (with a mean value of 21.2 ± 5.7 µg.kg^{-1}, 2SE, n=16, *Table 4*) and isotopic composition ranging from 17.6 and 31.0‰ (with a mean value of 24.8 ± 2,8‰, 2SE, n=14).

Table 4: B concentration (µg.kg^{-1}) and isotopic compositions (‰) in throughfall, stemflow and soil solutions collected at 5 chosen timeframes: 17/01/12 - 14/02/12 for winter, 10/04/12 - 09/05/12 for spring, 03/07/12 - 31/07/12 and 31/07/12 – 28/08/12 for summer and 24/09/12 - 22/10/12 for autumn.

Figure 3: Modelled B fluxes (µg.m^{-2}.d^{-1}, in black) and isotopic compositions (‰, in grey) in (a) throughfalls, (b) soil solutions at 0 cm, (c) -10 cm and (d) -30 cm. The line corresponds to the modelled values, the dots to the measured values and the shaded area to the associated uncertainties (1SD).

The corresponding calculated B fluxes are summarized in *Supplementary material Appendix 1, Table A.3* and *Figure 3*. Throughfall fluxes strongly vary over 2 orders of magnitude with values ranging from 3.7 µg.m^{-2}.d^{-1} to 103.6 µg.m^{-2}.d^{-1}. In soil solutions, fluxes vary between 8.3 and 114.3 µg.m^{-2}.d^{-1} in the humus layer (0 cm), between 1.7 and 69.6 µg.m^{-2}.d^{-1} at -10 cm and from 0.1 to 87.4 µg.m^{-2}.d^{-1} at -30 cm. All solution fluxes exhibit a bimodal evolution with higher values towards the end of Spring and during Autumn/Winter, and low (to very low) values during the summer.

3.8. Canopy leaching and humus mineralization

Using the data published in Roux et al. (2017) for F_{Aw} and R_{Aw}, we calculate a canopy leaching flux (F_{CL}) of 89.6 g.ha^{-1}.y^{-1} with an isotopic composition of 30.8‰ and a humus mineralization/litter leaching flux of 69.1 g.ha^{-1}.y^{-1} with an isotopic composition of 30.3‰ (*Table 2, Fig. 1*).

4. Discussion

4.1. Tracing B in water fluxes

Above- and under-ground water fluxes integrate multiple sources and biogeochemical mechanisms. In the following, we combine major elements with B contents and isotope to decipher the contribution of the different compartments of the soil/plant system to the B biogeochemical cycle.

4.1.1. Atmospheric inputs

Na and Cl are strongly correlated along the hydrological profile keeping a mass ratio close to the seawater value (*Fig. 4a*), which suggests that Na principally originates from atmospheric inputs and behaves conservatively along the water pathway. Since Na is not affected by canopy leaching, throughfalls integrate both wet atmospheric deposits and the soluble fraction of atmospheric dust deposits, including marine aerosols. The 2-fold increase in both Na and Cl concentrations observed directly under the canopy compared to rainfall only occur in winter and can therefore be attributed to a higher sea salt deposition (Roux et al., 2017). As waters pass through the humus and the mineral soil, Na concentrations remain equivalent to that of atmospheric inputs and therefore exhibit a conservative behavior when interacting with ground litter, humus layer and the different soil constituents. This is consistent with the very low Na concentration in the different litter samples and fresh leaves (respectively 0.13±0.03 and 0.07 $mg.kg^{-1}$), the low Na_2O content (<0.3% dry weight, *Supplementary material Appendix 1, Table A.4*) and overall lack of Na-bearing mineral phases (data not shown) in the soil. However, some soil solution samples at 0 cm and 30 cm deviate from the seawater line, possibly as a result of HCl gaseous deposition or fertilizers (Staelens et al., 2008; Roux et al., 2017). The lack of correlation between Cl and K in the throughfall samples rules out canopy leaching as a cause for Cl enrichment (Cole and Rapp, 1981).

4.1.2. From the canopy to the humus layer

Interactions with the canopy and the litter/humus layer leads to strong B enrichment in surface solutions (*Table 4*). The trends between B/Na and Ca/Na (*Fig 4b*), K/Na (*Fig 4c*) Si/Na (*Fig 4d*) and the seasonal evolution of B fluxes and isotopic compositions within the water-soil-plant system (*Fig 5)* emphasize (1) the primary control of vegetation over the B cycling like other macronutrients (e.g. Ca, Si, K) and (2) this enrichment varies in intensity for each element depending on seasonal activity and recycling process.

The B/Na molar ratio increases over one order of magnitude from 0.012 in rainfall to 0.09±0.02 (1SD, *Fig. 4*) in throughfalls with a significant increase of the B flux during the senescence period, which puts canopy leaching as a dominant source of B to the forest floor (*Fig. 5*). In parallel, K/Na, Ca/Na and Si/Na drastically increased in October from 0.2, 0.4 and 0.02 in rainfall (Roux et al., 2017) to 4.2±0.6, 1.9±0.8 and 0.62±0.08 (2SD) in throughfalls and 7.2, 0.95 and 0.78 in stemflows, respectively (*Fig. 4*). This evolution is accompanied by different trends between B/Na and Ca/Na in throughfalls and stemflows that could be explained by the influence of calcareous dust deposit on the canopy, common in this region of France and increases the Ca/Na in throughfalls (Lequy et al., 2013; Roux et al., 2017). However, this source remains of secondary importance for B as the range of $\delta^{11}B$ values within throughfalls/stemflows (18.9 - 37.2‰, *Table 4*) is incompatible with a significant contribution of dust particle leaching (340 $mg.kg^{-1}$, -0.3‰) in solutions (Roux et al., 2017).

As solutions pass through the humus layer, Ca and Si are further enriched with values as high as 16.8 for Ca/Na and 3.5 for Si/Na during summer (*Fig. 4b and d*). At the same time, both K/Na and B/Na increase from 0.040 ± 0.014 and 0.092 ± 0.014 (2SD) in throughfalls to 0.067 and 0.111 on the soil solutions, respectively (*Fig. 4c*). Litter decomposition is strongly influenced by environmental conditions and soil microfauna activity, which usually leads to high mineralization in Spring and Summer (d'Annunzio et al., 2008). However, elemental ratios and B flux significantly increase in October and February. Riotte et al. (2014) have suggested litter leaching to be the main process

controlling the elemental release on the forest floor, which is consistent with the B flux in soil solutions during senescence. Other studies have also shown microbial communities responsible for N fixation from complex organic molecules to be active from November to February (Kaiser et al., 2010, 2011), which is consistent with the relatively high TOC content observed in our study during this period (GW0: 18.5 – 25.2 $mg.L^{-1}$, *Supplementary material Appendix 1, Table A.5*).

Figure 4: Comparison between (a) Na ($mg.L^{-1}$) and Cl ($mg.L^{-1}$); (b) B/Na and Ca/Na; (c) K/Na and (d) Si/Na molar ratios in all water samples collected in the Montiers forest ecosystem. TF = throughfalls; SF = stemflow; Aw = atmospheric dissolved deposition (data from Roux et al, (2017)); GW0 = soil solution at 0 cm; GW10 = soil solution at -10 cm; GW30 = soil solution at -30 cm. lines represent linear fit to help identifying similarities of differences between sub-datasets (doesn't include Aw data).

4.1.3. Through the soil profile

B, Ca, Si and K show a relative depletion compared to Na in soil solutions from summer onward, resulting from the uptake by plant roots. Additionally, both B concentrations and isotopic compositions exhibit strong seasonal variations, especially under the root maximum density at -10cm. In the first 10 cm, $\delta^{11}B$ values exhibit a significant decrease as waters infiltrate soil layers in February and April, respectively from 24.1‰ to 17.6‰ and from 28.2‰ to 21.7‰.. In February, the significant decrease in both B concentrations and isotopic compositions cannot be explained by vegetation uptake processes as plants are in dormancy. Similar variations have been reported in another study who proposed dissolution/precipitation processes of poorly crystallized mineral phases leading to a ^{10}B removal in summer and input during winter (Cividini *et al.*, 2010). However, this appears inconsistent with our observations as soil solutions appear still under a tight control of biology-derived processes (no significant shift from their correlations with other major nutrient, *Fig. 4b, c and d*). A possible explanation could be the mineralization of fine roots whose turnover have been shown to be an important flux to the bulk soil every year (Turpault et al., 2018). While their mineralization rate isn't documented, some studies suggested lignin and cellulose degrading microbial communities to be active during winter (Kaiser et al., 2010, 2011) which is consistent with

526 the high TOC content, an indicator of soil organic matter degradation, in soil solutions during this
527 period (33.6 mg.kg^{-1}, *Supplementary material Appendix 1, Table A.4*). B role in bacterial development
528 has been suggested during N fixation processes and biofilm formation (Bolaños et al., 2004; Chen et
529 al., 2002). The development of bacterial communities could consume B in the first 10cm of the soil,
530 thereby explaining the B flux decrease, and in turn, lower the isotopic composition of the solution by
531 promoting fine root mineralization (-9.8‰, *Table 3*).

532 *Figure 5: Seasonal variability of B fluxes and isotopic compositions evolution along the*
533 *hydrological profile (from atmospheric dissolved deposition to soil solutions at -30 cm). Data from*
534 *atmospheric dissolved deposition are from Roux et al. (2017).*

535 ***4.1.4. B fluxes: an overwhelming biological control***

536 The systematic correlations observed in all compartments between B and strongly recycled
537 macronutrients (*Fig. 4*) as well as evolution of $\delta^{11}B$ values from throughfalls to soil solutions (*Fig. 5*)
538 allow using Eq. (2) – (7) to assign B to different fluxes of the biological cycle (*Table 2*). With an
539 integrated B flux of 313 g.ha^{-1}.y^{-1}, biology controls most of the B cycle of forested ecosystems: 159
540 g.ha^{-1}.y^{-1} transits as dissolved B either via canopy leaching (56%) or humus mineralization (44%), 72
541 g.ha^{-1}.y^{-1} are associated to litterfall and 82 g.ha^{-1}.y^{-1} are associated with fine root decay. When
542 compared to the beech stand B stock (571 g.ha^{-1}, Table 2), we observe that in 2012, the amount of B
543 released by vegetation corresponds to about 55% of the total B in perennial biomass. Consistently,
544 with an uptake flux of 276 g.ha^{-1}.y^{-1}, half of the B stock is being exchanged each year, with an almost
545 perfect balance between uptake and release by the vegetation. These values point to a very dynamic
546 biological cycle.

547 ***4.2. Boron isotope fractionation and implications for B mobility in forest ecosystem***

548 ***4.2.1. B distribution in plants: soluble and structural-bound pools***

549 Canopy leaching as well as early stage of biomass mineralization have in common to both
550 release the most soluble components (Adriaenssens et al., 2012; Berg, 2000; Staelens et al., 2008).
551 This results to a large release of B to solutions, preferentially ^{11}B as shown by the gradual decrease of

both B concentration and isotopic composition from the fresh leaves (26.1 mg.kg^{-1}, 23.5‰, *Table 3*) to the fresh litter in autumn (18.8 mg.kg^{-1}, 19.4‰, *Table 3*) and to the 2 litter layers on the forest floor (surface litter: 17.1 mg.kg^{-1}, 14.3‰; deep litter: 14.1 mg.kg^{-1}, 6.6‰, *Table 3*). A large fraction of B is therefore not bound to the cell wall, contrarily to what had been suggested by previous studies (Lehto et al., 2010b; González-Fontes et al., 2008). Structural-bound B therefore appears preferentially enriched in ^{10}B while soluble B would be enriched in ^{11}B. This observation is consistent with the findings of O'Neill et al. (2001) who showed that B stabilizes cell wall under its tetrahedral form, which accumulates the light isotope ^{10}B (Klochko et al., 2006). Speciation would therefore be the main parameter controlling B isotopic fractionation occurring during cell wall synthesis.

From the B isotopic ratios of leaf litter ($R_{leaf\ litter}$) and leaves (R_{leaf}), the progressive loss of soluble ^{11}B during canopy leaching is tentatively modeled by a Rayleigh-like distillation involving the isotopic fractionation caused by cell wall synthesis ($\alpha_{cell\ wall}$) and the mass fraction of the residual B after canopy leaching ($f_{leaf\ litter}$) as follows:

$$R_{leaf\ litter} = R_{leaf}\, f_{leaf\ litter}^{(\alpha_{cell\ wall}-1)} \quad (8)$$

Since the B budget in august leaves (114.2±7.5 g.ha-1, 23.5‰, *Supplementary material, Table A.1*) equals the sum of leaf litter and canopy leaching fluxes from August to December (122.4±8.2 g.ha-1, 27.6±3.4 ‰), then no B translocation between leaves and perennial biomass occur throughout the year. The isotopic ratio of the leaves can therefore be deduced from the B fluxes and isotopic ratios of leaf litter and throughfalls corrected from atmospheric inputs as follows:

$$F_{leaf} = F_{TF} - F_{Aw} + F_{leaf\ litter} \quad (9)$$

$$R_{leaf} \approx \frac{F_{TF} \times R_{TF} - F_{AW} \times R_{AW} + F_{leaf\ litter} \times R_{leaf\ litter}}{F_{TF} - F_{Aw} + F_{leaf\ litter}} \quad (10)$$

572 Combining Eq 8 and 10 to calculate the apparent isotopic fractionation factor caused by cell
573 wall synthesis gives $\alpha_{cell\ wall}$ = 0.9925±0.0045. This fractionation factor is much higher (closer to 1)
574 than expected by a speciation-driven mechanism at physiological pH 7-8 (α = 0.9728, Klochko et al.,
575 2006) indicating that the soluble B speciation is not the sole parameter at play.

576 ***4.2.2. B isotope fractionation during plant growth***

577 At the beech stand scale, the isotopic composition gradient observed from the deepest fine
578 roots (-11.7‰, *Table 3*) to the leaves (23.5‰, *Table 3*) reflects additional fractionation during
579 internal B transport. B is known to follow transpiration stream as exhibited by accumulation of
580 toxicity symptoms at the margin of leaves, where xylem vessels terminate (Oertli, 1993). This
581 transport can be facilitated by B specific channels shown to be most active in B deficiency conditions,
582 where B concentrations in the soil solutions are lower than the plant requirements (Shao et al., 2021;
583 Tanaka et al., 2008; Takano et al., 2002, 2006, 2010; Yoshinari and Takano, 2017). The B pathway
584 from the roots surface to the shoots includes at least three transmembrane processes: (i) import
585 from soil solutions to roots, (ii) export from roots to xylem and (iii) export from xylem to shoots
586 (Reid, 2014).

587 If we assume that the progressive transfer of B from the xylem to the surrounding tissues
588 along the root-to-shoot pathway follows a Rayleigh-like behaviour with a constant isotope
589 fractionation factor, then the B isotopic composition of the xylem evolves with its B removal as
590 follows:

$$R_{xylem} = R_{uptake} f^{\alpha_{xylem}-1} \quad (11)$$

591 With *f* the residual mass fraction of B in the xylem, α_{xylem} the isotopic fractionation during B transfer
592 from the xylem to the newly produced tissue and R_{uptake} the isotopic ratio of the B right after uptake

593 by tree roots. Here, we assume 1) a constant apparent B isotopic fractionation factor, which may
594 include a mechanism with multiple steps and 2) a single source of B entering the tree by the roots
595 and being progressively consumed during the xylem ascent up to the leaves. We also assume that
596 R_{uptake} is constant over time, which is supported by the rater constant $\delta^{11}B$ values in the soil solutions
597 shown in this study and in Cividini et al. (2010). If not constant, R_{uptake} should be considered as a
598 mean value integrated over the period of plant growth.

599 The B isotopic ratio of a growing compartment consuming B from f_1 to f_2 is given by:

$$\overline{R_i} = \frac{\alpha_{xylem} R_{uptake}}{f_2 - f_1} \times \int_{f_1}^{f_2} f^{\alpha_{xylem}-1} df \quad (12)$$

600 Were $\overline{R_i}$ is the averaged isotopic ratio of the tissues produced after consuming the amount of
601 B corresponding to the change of the remaining fractions from *f1* to *f2*. This gives after integration:

$$\overline{R_i} = \frac{R_{uptake}}{f_2 - f_1} \times ({f_2}^{\alpha_{xylem}} - {f_1}^{\alpha_{xylem}}) \quad (13)$$

602 Fine roots are the first tissue to take up B, so f_2 =1 and $f_1 = f_{fine\ roots}$

$$\overline{R_{fine\ roots}} = \frac{R_{uptake}}{1 - f_{fine\ roots}} \times \left(1 - {f_{fine\ roots}}^{\alpha_{xylem}}\right) \quad (14)$$

603 Leaves are the last tissue to take up B, so $f_2 = f_{leaves}$, the residual B fraction left by the other tissues,
604 and $f_1 = 0$.

$$\overline{R_{leaves}} = \frac{R_{uptake}}{f_{leaves}} \times ({f_{leaves}}^{\alpha_{xylem}}) \quad (15)$$

605 The B stock and isotopic composition of leaves are calculated as the sum of leaf litter and
606 throughfalls corrected from their atmospheric component as described in Eq. (9) and (10). Since our
607 data don't allow a precise determination of the B pathway between organs, the wood and bark
608 tissues are paired and considered homogenous. This includes the trunk and the large branches, for

609 which the bark has been analyses separately, whereas wood and bark have not been separated in
610 medium and fine branches.

611 This model was applied at two different scales. (i) Annually, where Eq. (14) and (15) are solved for
612 R_{uptake} and α_{xylem} only using data of leaves and fine roots to calculate the isotopic composition of the
613 intermediate tissues (branches and stem) grown during 2012 (*Fig 6a, b and c,* dotted line). (ii) A long-
614 term approach based on the bulk B stocks of the beech stand that integrate ≈ 50 years of growth,
615 where R_{uptake} and α_{xylem} are optimized to best fit all the B data measured in the different bulk organs
616 (*Fig. 6a, b and c,* full line). The hypotheses behind the long-term approach are that biomass has
617 grown with constant B distribution between organs and constant isotopic fractionation or that B
618 constantly exchanges between organs. None of these two hypotheses seems entirely satisfactory
619 with respect to our present knowledge of B functions in plants, but this approach is still considered
620 as a working hypothesis because of its agreement with our dataset (see discussion below). The
621 uncertainty on R_{uptake} and α_{xylem} was determined by Monte Carlo simulation based on the observed
622 variability of the mass fraction of B being transferred to each organ from roots to leaves and then
623 used to calculate the different *f* values. The results of these two approaches are reported in Table 5
624 and Fig 6.

625 The long-term approach can reproduce observed data to the exception of the fine roots,
626 which seem enriched in ^{10}B (*Fig. 6a and d, scenario 1*), and gives R_{uptake} = 6.3 ± 2.1‰ and α_{xylem} =
627 0.988 ± 0.003 (*Table 5*). A pool of coarse roots, which were not sampled in this study, has been
628 considered as an attempt to reconcile model and data, but has insignificant impact on the model
629 outputs (*Fig 6b and d*, *Table 5, scenario 2)*. For this calculation, the B stock in coarse roots was
630 extrapolated from biomass data (Turpault et al., 2018), the B concentration assumed similar to stem
631 wood ($[B]_{coarse\ roots}$ = 2.9 $mg.kg^{-1}$) and the B isotopic composition set as intermediate between fine
632 roots and stem ($\delta^{11}B_{coarse\ roots}$ = 0‰). Sensitivity tests around these extrapolations make the
633 contribution of coarse roots as a solution unlikely. An alternative explanation could be that the

dynamic fine roots pool, characterized by a rapid turnover 1.1 y^{-1} (Brunner et al., 2013; Finér et al., 2011; Montagnoli et al., 2012; Turpault et al., 2018), is subject to seasonal variations in B isotopes so that a single sampling is not representative of annual production. We calculate that the fine roots should have an annual B isotopic composition of -3‰ to make the entire dataset consistent with a Rayleigh-like B behaviour (*Fig. 6c and 6f, scenario 3*). This scenario gives R_{uptake} = 7.0 ± 2.1 ‰ and α_{xylem} = 0.990 ± 0.002, not much different from outputs of scenario 1. Here again, consideration of large roots has no impact on the calculated R_{uptake} and α_{xylem} values.

Table 5: Results of the Rayleigh like model for B during plant growth

Figure 6: Results of the Rayleigh like model for B during plant growth. (a) corresponds to the annual and long-term modeling using raw data (scenario 1). (b) adds an hypothetical B stock in coarse roots based on data from Turpault et al, (2018) (scenario 2). (c) changes the $\delta^{11}B$ value of the fine root compartment to make the entire dataset consistent with Rayleigh-like behavior ($\delta^{11}B_{fine\ roots}$ = -3‰; scenario 3). (d), (e) and (f) compare the results of modelled value of annually formed biomass to the measured value in bulk intermediate organs (branches and stem) for each scenario.

The annual approach, based on fines roots and leaves, only assumes that B is distributed and isotopically fractionated between fresh tissues using the biomass annual growth data (*Table 3*). Here, no B transfer between old and young tissues is considered. This allows to calculate the B isotopic composition of the newly produced intermediate organs (stem and branches) that can then be compared to their respective measured bulk values. This approach gives R_{uptake} = 11.9 ± 7.5‰ and α_{xylem} = 0.975 ± 0.010, different from those calculated with bulk biomass (see *Table 5 and Fig. 6, scenario 1*). These calculated values are not significantly different under scenario 2 but increase to R_{uptake} = 14.0 ± 7.1‰ and α_{xylem} = 0.980 ± 0.009 when fine roots are set at $\delta^{11}B$ = -3‰ (*scenario 3, Table 5*). Following the Rayleigh model, the discrepancy shown by these two approaches makes difficult to explain B isotopes in the perennial biomass from data of the annual products. Explanations may be found in a preferential ^{11}B redistribution within perennial biomass via boric acid transporters, as suggested by Shao et al., (2021) and Tanaka et al., (2008). Environmental changes, such as atmospheric pollution could also lead to ^{10}B enrichment of the recent biomass products

(Guinoiseau et al., 2018; Roux et al., 2017). Further research on B isotopes in soil/plant interactions as well as in different part of the wood is still needed to help clarify this point.

Regardless of the chosen approach, the model puts vegetation as the main driver of isotopic composition increase observed between soil and leaves, most likely induced by B internal allocation and transport network. The magnitude of this increase is therefore dictated by the amount of B allocated to fine roots and perennial tissues, which accumulate ^{10}B. The model also points to additional mechanisms occurring on a longer timescale as shown by the differences between long-term and annual apparent fractionation factors. Calculated α_{xylem} varies from 0.975 ± 0.010 for the annual products to 0.988 ± 0.003 for the bulk biomass. Translocation processes have been mentioned in previous studies, where channels involved in xylem-phloem transfer allow boric acid, enriched in ^{11}B, distribution to growing tissue (e.g. Tanaka et al., 2008).

4.2.3. Boron isotope fractionation during vegetation uptake

Cividini et al, (2010) estimated the apparent isotopic fractionation factor induced by vegetation uptake to be of relatively low magnitude in the Strengbach catchment ($0.990 < \alpha_{uptake} < 1$). This was mostly based on the drastic decrease in B concentrations in soil solutions at roots depth without any significant shift in $\delta^{11}B$ values. In this study however, comparing the calculated annual R_{uptake} to the isotopic composition of soil solutions allows us to give a more representative value since it solely results from the passage of B from soil solution to root xylem, provided that roots take up B from gravitational waters rather than porous water (Goldberg, 1997). The soil solutions in the maximum root density zone (0 – 10 cm) during peak vegetation activity (from March to September) exhibit a weighed mean value of 27.7‰, which limits the range of possible α_{uptake} values to 0.979 - 0.994. This value is much higher than previously reported, but consistent with preferential absorption of ^{10}B, especially in deficiency conditions (Cividini et al., 2010; Geilert et al., 2019). Alternatively, the low B isotopic ratio calculated for R_{uptake} may reflect the contribution of at least

686 another source than gravitational waters, which could be found in the pool of B adsorbed on soil
687 minerals. If so, R_{uptake} would reflect reflect the bioavailable reserve of B in the soil.

688 The lack of observed effect of the high uptake flux (276 g.ha^{-1}.y^{-1}) on the δ^{11}B with depth
689 implies a constant and large source of isotopically low B. The systematic correlations observed
690 between dissolved B and strongly recycled macronutrients doesn't point to a major influence of soil
691 mineralogical constituents on soil solution chemistry. Rather, fine roots pool have been shown to be
692 a dynamic soil nutrient pool, including in our study site (Turpault et al., 2018), putting them as the
693 most likely source of B in soils. It is then surprising that overall limited seasonal and vertical δ^{11}B
694 variations in soil solutions actually hide such a dynamic turnover. This is partly due to the buffering
695 capacity of throughfalls and stemflows, which are a significant source of B with high δ^{11}B to soil
696 solutions. Nevertheless, this implies to revaluate the mechanism of fine roots mineralization, in
697 particular their contribution to the belowground B budget as well as the B pathway from dead to
698 living fines roots without visible influence on the soil water chemistry. Unfortunately, the lack of
699 information about fine root mineralization dynamics and the concomitant isotope fractionation
700 occurring between the different B pools (structural vs soluble) makes evaluating the contribution of
701 fine roots challenging and unconstrained.

702 *5. Summary and perspectives*

703 Soils constitute the largest B reservoir at the ecosystem scale (245 kg.ha^{-1}; -6.9‰). However,
704 even if soil B is mostly controlled by the B-rich and highly reactive clay phase, our results confirm the
705 control of biology-related processes on the B cycle in forest ecosystem (canopy exchange 90 g.ha^{-1}.y^{-}
706 ^{1}, litterfall 72 g.ha^{-1}.y^{-1} and litter leaching/organic matter mineralisation 69 g.ha^{-1}.y^{-1}). In 2012, 276
707 g.ha^{-1} out of the 571 g.ha^{-1} total B-bound perennial biomass has been renewed, thus showing the
708 extreme reactivity of the vegetation pool with respect to B. The strong biological imprint on the B
709 cycle is highlighted by the ^{11}B enriched isotopic compositions of the solutions compared to the
710 mineral source, but most importantly by the systematic correlations observed in all compartments

between B and strongly recycled elements (Ca, K and Si). While the correlation of B with K highlights the vegetation cycling with clear release/uptake periods, correlations with Ca and Si show different patterns of nutrient release depending on the considered mechanism (litter leaching/organic matter mineralisation or canopy exchange), probably as a result of B incorporation into structural or soluble part of the leaves. This partitioning, most likely due to cell wall synthesis, is further observed with B isotopes, which exhibit an apparent fractionation factor between structural and soluble forms of 0.9925 ± 0.0045.

The large isotopic composition gradient observed between deeper fine roots (-11.2‰) and leaves (23.5‰) is consistent with a Rayleigh-like model leading to ^{11}B enrichment in the leaves, whose magnitude is dependent on the production of perennial biomass. This shows that plant internal transport and the allocation of resources is responsible for the large isotopic composition differences observed in previous studies between leaves and soils. Nevertheless, differences are observed depending on whether the annual (α_{xylem} = 0.980 ± 0.009) or total biomass is considered (α_{xylem} of 0.990 ± 0.002), suggesting ^{11}B transfer from old to new tissue within perennial tissue.

The Rayleigh model also points to an apparent isotopic fractionation factor induced by vegetation uptake much higher than previously thought ($0.979 < \alpha_{uptake} < 0.994$). Surprisingly, soil solutions don't exhibit any increase in $\delta^{11}B$ with depth, implying a dynamic isotopically low B source, which is hypothesized to be fine roots since soil mineralogical constituents appear to have a limited influence. Despite the buffering capacity of stemflow and throughfalls, it is surprising that rather limited seasonal and vertical $\delta^{11}B$ variations in soil solutions actually hide such distinct and dynamic processes. This implies to revaluate the way fine roots are considered in the belowground budget calculation and the cycling of dead biomass.

Beyond reconciliating the large differences in terms of isotopic compositions between vegetation and bulk soil, which have remained unclear and/or unconstrained to this day (Gaillardet and Lemarchand, 2018; Cividini et al., 2010; Chetelat et al., 2021), this model highlights how B

isotopes could give insight in the status of nutrients and evolution of forest ecosystems. Annual and long-term parameters provided by the model have shown to be significantly different due to mechanisms occurring at different timescale with annual tissue representative of the ecosystem's current status, and perennial tissue representative of its evolution. While this statement may appear unsurprising to some, such an approach has never been put forward for micronutrients critical in plant development such as B. Since B internal transport, including the accumulation in woody tissue, leads to an overall ^{11}B enrichment of the ecosystem, therefore simple, easy-to-access parameters, such as the $\delta^{11}B$ difference between soil and leaves ($\Delta^{11}B_{soil\text{-}leaves}$), branches ($\Delta^{11}B_{soil\text{-}branches}$), or stem ($\Delta^{11}B_{soil\text{-}stem}$) could be used to evaluate of the allocation and/or accumulation of resources.

Nevertheless, in his current state, the model fails to explain why the beech stand still exhibit higher values than the soil it originates from ($\Delta^{11}B_{beech\ stand\text{-}soil}$ = 12‰). However, high biological fluxes combined with the ^{11}B enrichment caused by internal B transport completely overrun the lower isotopic composition sources such as weathering. This slow shift towards higher values could therefore be the result of the intensity of the biological cycle over the geologic inputs (atmospheric deposition and weathering).

Acknowledgement

We thank the ONF (Office National des Forêts) who accepted the site installation, the Region Lorraine and Andra (French national radioactive waste management agency) for supporting us during the implementation of this article and financing the scholarship of PR. We would also thank the Andra and INRAE personnel (Carine Cochet and Claire Pantigny) for the continuous sampling during this study; Christophe Calvaruso for the database management; Serge Didier for site implementation and management; Laurent Saint-André, Laura Franoux and Astrid Genêt for the development of allometric equations; Claire Pantigny, Louisette Gelhaye, Bruno Simon, Claude Nys, Jonathan Mangin, Céline Goldstein, Frédérique César, Maëlle D'Arbaumont and Maxime Simon for technical help.

Tables and Figures

Table 1: Definitions for equation and system components

Equation components	
R	Isotopic ratio
F	Flux
α	Isotopic fractionation factor
System components	
CL	Canopy leaching
TF	Throughfall
SF	Stemflow
Aw	Atmospheric dissolved deposition
hum_min	Humus mineralization
upt	Vegetation uptake
0cm	Solutions at 0cm depth
Litterfall	Litterfall
cycling	SF + TF + Litterfall
growth	Perenial biomass growth

766 *Table 2: B stocks (g.ha^{-1}). yearly flux (g.ha^{-1}. y^{-1}) and isotopic compositions (‰) constituting the B*
767 *biogeochemical cycle in the Montiers temperate forest ecosystem*

Compartment	**B**	**δ^{11}B**
Stocks	*g.ha^{-1}*	*‰*
Soil	**135 x 10^3**	*-6.9*
Humus	**173**	*6.7*
Vegetation		
- Perennial	**571 ± 119**	*5.0 ± 2.0*
- Leaves	**114**	*23.5*
- Fine roots	**74**	*-9.3*
Fluxes	*g.ha^{-1}.y^{-1}*	*‰*
Litterfall	**72**	*17.3*
Throughfalls	**98 ± 6**	*29.1 ± 2.8*
Stemflows	**9 ± 0**	*31.1 ± 0.3*
Drainage 0cm	**176 ± 6**	*29.7 ± 1.6*
Drainage -10cm	**121 ± 6**	*25.7 ± 2.0*
Drainage -30cm	**109 ± 27**	*23.7 ± 10.5*
Exportation residuals	**10**	*8.4*
Exportation harvest	**17**	*3.0*
Fine root decay	**82**	*-9.3*
Canopy exchange	**90**	*30.8*
Humus mineralization	**69**	*30.3*
Vegetation uptake	**276**	-
Perennial growth	**33**	-

768

769

770

771

772 *Table 3: B concentration (mg.kg^{-1}) and isotopic composition (‰) of soil, soil constituents, humus,*
773 *beech stand and litter samples collected in the Montiers forest ecosystem.*

Sample name	Sample type	Sampling date	B	$\delta^{11}B$
Soil samples			*mg.kg^{-1}*	*‰*
Surf Lit	Surface litter	Spring 2012	**17.1**	14.3
Deep Lit	Deep litter	Spring 2012	**14.8**	6.6
Hum	humus	June 2010	**18.6**	6.7
Soil 0-5	Soil horizon 0-5cm	March 2011	**54.6**	-6.7
Soil 5-15	Soil horizon 5-15cm	March 2011	**63.3**	-6.9
Soil 15-30	Soil horizon 15-30cm	March 2011	**82.8**	-7.1
Soil 30 - 135	Soil horizon 30-135cm	March 2011	**75.5**	-6.8
Soil >135	Soil horizon >135cm	March 2011	**42.4**	-6.1
Clay	Decarbonated clay	March 2011	**220.0**	-5.0
Limestone	Limestone bedrock	March 2011	**8.2**	-5.4
Beech stand				
Lf	Leaves	28/08/2012	**26.1**	23.5
B<4a	Branch <4cm	Winter 2009	**12.1**	*8.2*
B<4b	Branch <4cm	Winter 2009	**12.2**	*13.6*
B<4c	Branch <4cm	Winter 2009	**11.7**	*10.9*
B<4d	Branch <4cm	Winter 2009	**10.9**	*6.7*
B 4-7a	Branch 4-7cm	Winter 2009	**6.8**	*7.5*
B 4-7b	Branch 4-7cm	Winter 2009	**5.9**	*5.6*
B 4-7c	Branch 4-7cm	Winter 2009	**5.3**	*3.5*
B 4-7d	Branch 4-7cm	Winter 2009	**5.7**	*4.9*
BW>7a	Branch wood >7cm	Winter 2009	**2.8**	*7.8*
BW>7b	Branch wood >7cm	Winter 2009	**3.2**	*5.4*
BW>7c	Branch wood >7cm	Winter 2009	**2.4**	*0.2*
BW>7d	Branch wood >7cm	Winter 2009	**3.1**	*4.1*
BB>7a	Branch bark >7cm	Winter 2009	**33.1**	*10.3*
BB>7b	Branch bark >7cm	Winter 2009	**25.9**	*10.7*
BB>7c	Branch bark >7cm	Winter 2009	**26.0**	*3.8*
BB>7d	Branch bark >7cm	Winter 2009	**29.3**	*9.3*
SWa	Stem wood	Winter 2009	**2.4**	*2.0*
SWb	Stem wood	Winter 2009	**2.5**	*3.1*
SWc	Stem wood	Winter 2009	**2.4**	*-0.9*
SWd	Stem wood	Winter 2009	**2.5**	*1.5*
SBa	Stem bark	Winter 2009	**33.6**	*4.7*
SBb	Stem bark	Winter 2009	**21.0**	*5.3*
SBc	Stem bark	Winter 2009	**24.9**	*1.5*
SBd	Stem bark	Winter 2009	**31.5**	*4.4*
R 0-15	Root 0-5cm	March 2011	**12.2**	-7.2
R 5-15	Root 5-15cm	March 2011	**9.2**	-11.7
Litterfall				
LL win	Leaf litter	21/12/11 - 13/03/12	**16.0**	*13.7*
LL spr	Leaf litter	13/03/12 - 05/06/12	**15.3**	*6.9*
LL sum	Leaf litter	05/06/12 - 28/08/12	**17.1**	*21.3*
LL win	Leaf litter	28/08/12 - 18/12/12	**18.8**	*19.4*

LW win	Wood litter	21/12/11 - 13/03/12	**16.0**	-0.2
LW spr	Wood litter	13/03/12 - 05/06/12	**16.0**	6.9
LW sum	Wood litter	05/06/12 - 28/08/12	**22.4**	3.1
LW aut	Wood litter	28/08/12 - 18/12/12	**11.9**	5.8
LO win	Other litter	21/12/11 - 13/03/12	**20.0**	1.4
LO spr	Other litter	13/03/12 - 05/06/12	**12.0**	9.0
LO sum	Other litter	05/06/12 - 28/08/12	**12.4**	11.6
LO aut	Other litter	28/08/12 - 18/12/12	**5.6**	11.9

774

775

776

Table 4: B concentration (µg.kg^{-1}) and isotopic compositions (‰) in throughfall, stemflow and soil solutions collected at 5 chosen timeframes: 17/01/12 - 14/02/12 for winter, 10/04/12 - 09/05/12 for spring, 03/07/12 - 31/07/12 and 31/07/12 – 28/08/12 for summer and 24/09/12 - 22/10/12 for autumn.

Sample name	**Sample type**	**Sampling date**	**B**	**$\delta^{11}B$**
			µg.kg^{-1}	*‰*
TF1 Win	Throughfall	17/01/12 - 14/02/12	**4.6**	*20.1*
TF2 Win	Throughfall	17/01/12 - 14/02/12	**2.7**	*20.6*
TF3 Win	Throughfall	17/01/12 - 14/02/12	**5.1**	*25.5*
TF2 Spr	Throughfall	10/04/12 - 09/05/12	**5.3**	*18.8*
TF2 Spr	Throughfall	10/04/12 - 09/05/12	**7.2**	*19.0*
TF2 Spr	Throughfall	10/04/12 - 09/05/12	**3.8**	*22.2*
TF1 Sum	Throughfall	03/07/12 - 31/07/12	**9.7**	*31.8*
TF2 Sum	Throughfall	03/07/12 - 31/07/12	**6.4**	*32.1*
TF1 Sum2	Throughfall	31/07/12 - 28/08/12	**11.7**	*31.0*
TF2 Sum2	Throughfall	31/07/12 - 28/08/12	**10.5**	*31.2*
TF1 Aut	Throughfall	25/09/12 - 23/10/12	**9.3**	*35.7*
TF2 Aut	Throughfall	25/09/12 - 23/10/12	**11.0**	*37.2*
TF3 Aut	Throughfall	25/09/12 - 23/10/12	**6.3**	*33.6*
SF Win	Stemflow	17/01/12 - 14/02/12	**6.8**	*26.7*
SF Spr	Stemflow	10/04/12 - 09/05/12	**6.4**	*27.1*
SF Sum	Stemflow	03/07/12 - 31/07/12	**27.9**	*32.3*
SF Sum2	Stemflow	31/07/12 - 28/08/12	**38.3**	*30.2*
SF Aut	Stemflow	25/09/12 - 23/10/12	**13.6**	*34.7*
GW0 Win	Groundwater 0cm	17/01/12 - 14/02/12	**15.3**	*24.1*
GW0 Spr	Groundwater 0cm	10/04/12 - 09/05/12	**12.1**	*28.2*
GW0 Sum	Groundwater 0cm	03/07/12 - 31/07/12	**16.5**	*27.1*
GW0 Sum2	Groundwater 0cm	31/07/12 - 28/08/12	**22.4**	*30.8*
GW0 Aut	Groundwater 0cm	25/09/12 - 23/10/12	**18.6**	*30.6*
GW10 Win	Groundwater 10cm	17/01/12 - 14/02/12	**7.4**	*17.6*
GW10 Spr	Groundwater 10cm	10/04/12 - 09/05/12	**14.7**	*21.7*
GW10 Sum	Groundwater 10cm	03/07/12 - 31/07/12	**17.4**	*25.7*
GW10 Sum2	Groundwater 10cm	31/07/12 - 28/08/12	**19.2**	*31.0*
GW10 Aut	Groundwater 10cm	25/09/12 - 23/10/12	**18.0**	*30.8*
GW30 Win	Groundwater 30cm	17/01/12 - 14/02/12	**24.0**	*18.4*
GW30 Spr	Groundwater 30cm	10/04/12 - 09/05/12	**13.6**	*18.8*
GW30 Sum2	Groundwater 30cm	31/07/12 - 28/08/12	**28.5**	*17.7*
GW30 Aut	Groundwater 30cm	25/09/12 - 23/10/12	**11.3**	*24.3*

783

784

785 *Table 5: Results of the Rayleigh like model for B during plant growth*

	Scenario 1		Scenario 2		Scenario 3	
	R_{uptake}	α_{xylem}	R_{uptake}	α_{xylem}	R_{uptake}	α_{xylem}
Long term	6.3±2.1	0.988±0.003	6.3±2.1	0.989±0.002	7.0±2.1	0.990±0.002
Annual	11.9±7.5	0.975±0.010	11.4±7.3	0.976±0.010	14.0±7.1	0.980±0.009

786

787

References

Adriaenssens, S., Hansen, K., Staelens, J., Wuyts, K., De Schrijver, A., Baeten, L., Boeckx, P., Samson, R., Verheyen, K., 2012. Throughfall deposition and canopy exchange processes along a vertical gradient within the canopy of beech (Fagus sylvatica L.) and Norway spruce (Picea abies (L.) Karst). Sci. Total Environ. 420, 168–182.

Berg, B., 2000. Litter decomposition and organic matter turnover in northern forest soils. For. Ecol. Manage. 133, 13–22.

Blevins, D.G., Lukaszewski, K.M., 1998. Boron in plant structure and function. Annu. Rev. Plant Biol. 49, 481–500.

Bolaños, L., Lukaszewski, K., Bonilla, I., Blevins, D., 2004. Why boron? Plant Physiol. Biochem. 42, 907–912.

Brown, P.H., Bellaloui, N., Wimmer, M.A., Bassil, E.S., Ruiz, J., Hu, H., Pfeffer, H., Dannel, F., Römheld, V., 2002. Boron in plant biology. Plant Biol. 4, 205–223.

Brunner, I., Bakker, M.R., Björk, R.G., Hirano, Y., Lukac, M., Aranda, X., Børja, I., Eldhuset, T.D., Helmisaari, H.S., Jourdan, C., Konôpka, B., López, B.C., Miguel Pérez, C., Persson, H., Ostonen, I., 2013. Fine-root turnover rates of European forests revisited: an analysis of data from sequential coring and ingrowth cores. Plant Soil 362, 357–372. https://doi.org/10.1007/s11104-012-1313-5

Calvaruso, C., Kirchen, G., Saint-André, L., Redon, P.-O., Turpault, M.-P., 2017. Relationship between soil nutritive resources and the growth and mineral nutrition of a beech (Fagus sylvatica) stand along a soil sequence. CATENA 155, 156–169. https://doi.org/https://doi.org/10.1016/j.catena.2017.03.013

Chen, X., Schauder, S., Potier, N., Van Dorsselaer, A., Pelczer, I., Bassler, B.L., Hughson, F.M., 2002. Structural identification of a bacterial quorum-sensing signal containing boron. Nature 415, 545–549.

Chetelat, B., Gaillardet, J., Chen, J. Bin, 2021. Dynamic of boron in forest ecosystems traced by its isotopes: A modeling approach. Chem. Geol. 560, 119994. https://doi.org/10.1016/j.chemgeo.2020.119994

Cividini, D., Lemarchand, D., Chabaux, F., Boutin, R., Pierret, M.C., 2010. From biological to lithological control of the B geochemical cycle in a forest watershed (Strengbach, Vosges). Geochim. Cosmochim. Acta 74, 3143–3163.

Cole, D.W., Rapp, M., 1981. Elemental cycling in forest ecosystems. Dyn. Prop. For. Ecosyst. 23, 341–409.

d'Annunzio, R., Zeller, B., Nicolas, M., Dhôte, J.-F., Saint-André, L., 2008. Decomposition of European beech (Fagus sylvatica) litter: Combining quality theory and 15N labelling experiments. Soil Biol. Biochem. 40, 322–333. https://doi.org/https://doi.org/10.1016/j.soilbio.2007.08.011

Dincher, M., Calvaruso, C., Turpault, M.-P., 2020. Major element residence times in humus from a beech forest: The role of element forms and recycling. Soil Biol. Biochem. 141, 107674. https://doi.org/https://doi.org/10.1016/j.soilbio.2019.107674

Fantle, M.S., DePaolo, D.J., 2004. Iron isotopic fractionation during continental weathering. Earth Planet. Sci. Lett. 228, 547–562. https://doi.org/https://doi.org/10.1016/j.epsl.2004.10.013

Finér, L., Ohashi, M., Noguchi, K., Hirano, Y., 2011. Factors causing variation in fine root biomass in forest ecosystems. For. Ecol. Manage. 261, 265–277. https://doi.org/10.1016/j.foreco.2010.10.016

Gaillardet, J., Lemarchand, D., 2018. Boron in the Weathering Environment, in: Boron Isotopes. Springer, pp. 163–188.

Geilert, S., Vogl, J., Rosner, M., Eichert, T., 2019. Boron isotope variability related to boron speciation (change during uptake and transport) in bell pepper plants and SI traceable n(11B)/n(10B) ratios for plant reference materials. Rapid Commun. Mass Spectrom. 33, 1137–1147. https://doi.org/https://doi.org/10.1002/rcm.8455

Goldberg, S., 1997. Reactions of boron with soils. Plant Soil 193, 35–48.

González-Fontes, A., Rexach, J., Navarro-Gochicoa, M.T., Herrera-Rodríguez, M.B., Beato, V.M., Maldonado, J.M., Camacho-Cristóbal, J.J., 2008. Is boron involved solely in structural roles in vascular plants. Plant Signal Behav 3, 24–26.

Granier, A., Bréda, N., Biron, P., Villette, S., 1999. A lumped water balance model to evaluate duration and intensity of drought constraints in forest stands. Ecol. Modell. 116, 269–283. https://doi.org/https://doi.org/10.1016/S0304-3800(98)00205-1

Guinoiseau, D., Louvat, P., Paris, G., Chen, J.-B., Chetelat, B., Rocher, V., Guérin, S., Gaillardet, J., 2018. Are boron isotopes a reliable tracer of anthropogenic inputs to rivers over time? Sci. Total Environ. 626, 1057–1068.

Gupta, U.C., 1993. Boron and its role in crop production. CRC press.

Henry, M., Picard, N., Trotta, C., Manlay, R., Valentini, R., Bernoux, M., Saint André, L., 2011. Estimating tree biomass of sub-Saharan African forests: a review of available allometric equations. Silva Fenn. 45, 477–569.

Hu, Z., Gao, S., 2008. Upper crustal abundances of trace elements: A revision and update. Chem. Geol. 253, 205–221. https://doi.org/https://doi.org/10.1016/j.chemgeo.2008.05.010

Kaiser, C., Fuchslueger, L., Koranda, M., Gorfer, M., Stange, C.F., Kitzler, B., Rasche, F., Strauss, J., Sessitsch, A., Zechmeister-Boltenstern, S., 2011. Plants control the seasonal dynamics of microbial N cycling in a beech forest soil by belowground C allocation. Ecology 92, 1036–1051.

Kaiser, C., Koranda, M., Kitzler, B., Fuchslueger, L., Schnecker, J., Schweiger, P., Rasche, F., Zechmeister-Boltenstern, S., Sessitsch, A., Richter, A., 2010. Belowground carbon allocation by trees drives seasonal patterns of extracellular enzyme activities by altering microbial community composition in a beech forest soil. New Phytol. 187, 843–858.

Kimmig, S.R., Holmden, C., Bélanger, N., 2018. Biogeochemical cycling of Mg and its isotopes in a sugar maple forest in Québec. Geochim. Cosmochim. Acta 230, 60–82. https://doi.org/https://doi.org/10.1016/j.gca.2018.03.020

Kirchen, G., Calvaruso, C., Granier, A., Redon, P.-O., Van der Heijden, G., Bréda, N., Turpault, M.-P., 2017. Local soil type variability controls the water budget and stand productivity in a beech forest. For. Ecol. Manage. 390, 89–103. https://doi.org/https://doi.org/10.1016/j.foreco.2016.12.024

Klochko, K., Kaufman, A.J., Yao, W., Byrne, R.H., Tossell, J.A., 2006. Experimental measurement of boron isotope fractionation in seawater. Earth Planet. Sci. Lett. 248, 276–285.

870 Kot, F.S., Farran, R., Fujiwara, K., Kharitonova, G. V, Kochva, M., Shaviv, A., Sugo, T., 2016. On boron
871 turnover in plant–litter–soil system. Geoderma 268, 139–146.
872 https://doi.org/http://dx.doi.org/10.1016/j.geoderma.2016.01.022

873 Lehto, T., Aphalo, P.J., Saranpää, P., Laakso, T., Smolander, A., 2010a. Decomposition and element
874 concentrations of Norway spruce needle litter with differing B, N, or P status. Plant Soil 330,
875 225–238.

876 Lehto, T., Smolander, A., Aphalo, P.J., 2010b. Decomposition and element concentrations of silver
877 birch leaf litter as affected by boron status of litter and soil. Plant Soil 329, 195–208.

878 Lemarchand, D., Cividini, D., Turpault, M.P., Chabaux, F., 2012. Boron isotopes in different grain size
879 fractions: Exploring past and present water–rock interactions from two soil profiles
880 (Strengbach, Vosges Mountains). Geochim. Cosmochim. Acta 98, 78–93.
881 https://doi.org/https://doi.org/10.1016/j.gca.2012.09.009

882 Lemarchand, D., Gaillardet, J., 2006. Transient features of the erosion of shales in the Mackenzie
883 basin (Canada), evidences from boron isotopes. Earth Planet. Sci. Lett. 245, 174–189.
884 https://doi.org/https://doi.org/10.1016/j.epsl.2006.01.056

885 Lemarchand, D., Gaillardet, J., Lewin, E., Allegre, C.J., 2000. The influence of rivers on marine boron
886 isotopes and implications for reconstructing past ocean pH. Nature 408, 951–954.

887 Lemarchand, E., Schott, J., Gaillardet, J., 2007. How surface complexes impact boron isotope
888 fractionation: Evidence from Fe and Mn oxides sorption experiments. Earth Planet. Sci. Lett.
889 260, 277–296.

890 Lequy, É., Legout, A., Conil, S., Turpault, M.-P., 2013. Aeolian dust deposition rates in Northern
891 French forests and inputs to their biogeochemical cycles. Atmos. Environ. 80, 281–289.
892 https://doi.org/https://doi.org/10.1016/j.atmosenv.2013.07.075

893 Marentes, E., Vanderpool, R.A., Shelp, B.J., 1997. Boron-isotope fractionation in plants. Can. J. Plant
894 Sci. 77, 627–629.

895 Miwa, K., Fujiwara, T., 2010. Boron transport in plants: Co-ordinated regulation of transporters. Ann.
896 Bot. 105, 1103–1108.

897 Montagnoli, A., Terzaghi, M., Di Iorio, A., Scippa, G.S., Chiatante, D., 2012. Fine-root seasonal pattern,
898 production and turnover rate of European beech (Fagus sylvatica L.) stands in Italy Prealps:
899 possible implications of coppice conversion to high forest. Plant Biosyst. Int. J. Deal. with all Asp.
900 Plant Biol. 146, 1012–1022.

901 Noireaux, J., Sullivan, P.L., Gaillardet, J., Louvat, P., Steinhoefel, G., Brantley, S.L., 2021. Developing
902 boron isotopes to elucidate shale weathering in the critical zone. Chem. Geol. 559, 119900.
903 https://doi.org/https://doi.org/10.1016/j.chemgeo.2020.119900

904 O'Neill, M.A., Eberhard, S., Albersheim, P., Darvill, A.G., 2001. Requirement of borate cross-linking of
905 cell wall rhamnogalacturonan II for Arabidopsis growth. Science (80-.). 294, 846–849.

906 Oertli, J.J., 1993. The mobility of boron in plants, in: Plant Nutrition—from Genetic Engineering to
907 Field Practice. Springer, pp. 393–396.

908 Opfergelt, S., Williams, H.M., Cornelis, J.T., Guicharnaud, R.A., Georg, R.B., Siebert, C., Gislason, S.R.,
909 Halliday, A.N., Burton, K.W., 2017. Iron and silicon isotope behaviour accompanying weathering
910 in Icelandic soils, and the implications for iron export from peatlands. Geochim. Cosmochim.

911 Acta 217, 273–291. https://doi.org/https://doi.org/10.1016/j.gca.2017.08.033

912 Ozturk, Munir, Sakcali, S., Gucel, S., Tombuloglu, H., 2010. Boron and Plants, in: Ashraf, M., Ozturk,
913 M, Ahmad, M.S.A. (Eds.), Plant Adaptation and Phytoremediation. Springer Netherlands,
914 Dordrecht, pp. 275–311. https://doi.org/10.1007/978-90-481-9370-7_13

915 Park, H., Schlesinger, W.H., 2002. Global biogeochemical cycle of boron. Global Biogeochem. Cycles
916 16, 20–21.

917 Prunier, J., Chabaux, F., Stille, P., Gangloff, S., Pierret, M.C., Viville, D., Aubert, A., 2015. Geochemical
918 and isotopic (Sr, U) monitoring of soil solutions from the Strengbach catchment (Vosges
919 mountains, France): Evidence for recent weathering evolution. Chem. Geol. 417, 289–305.
920 https://doi.org/https://doi.org/10.1016/j.chemgeo.2015.10.012

921 Reid, R., 2014. Understanding the boron transport network in plants. Plant Soil 385, 1–13.
922 https://doi.org/10.1007/s11104-014-2149-y

923 Riotte, J., Maréchal, J.C., Audry, S., Kumar, C., Bedimo, J.P.B., Ruiz, L., Sekhar, M., Cisel, M., Tarak,
924 R.C., Varma, M.R.R., 2014. Vegetation impact on stream chemical fluxes: Mule Hole watershed
925 (South India). Geochim. Cosmochim. Acta 145, 116–138.

926 Rose, E.F., Chaussidon, M., France-Lanord, C., 2000. Fractionation of boron isotopes during erosion
927 processes: the example of Himalayan rivers. Geochim. Cosmochim. Acta 64, 397–408.

928 Rosner, M., Pritzkow, W., Vogl, J., Voerkelius, S., 2011. Development and validation of a method to
929 determine the boron isotopic composition of crop plants. Anal. Chem. 83, 2562–2568.
930 https://doi.org/10.1021/ac102836h

931 Roux, P., Lemarchand, D., Hughes, H.J., Turpault, M.-P., 2015. A Rapid Method for Determining Boron
932 Concentration (ID-ICP-MS) and δ11B (MC-ICP-MS) in Vegetation Samples after Microwave
933 Digestion and Cation Exchange Chemical Purification. Geostand. Geoanalytical Res. 39, 453–
934 466. https://doi.org/10.1111/j.1751-908X.2014.00328.x

935 Roux, P., Turpault, M.-P., Kirchen, G., Redon, P.-O., Lemarchand, D., 2017. Boron Dissolved and
936 Particulate Atmospheric Inputs to a Forest Ecosystem (Northeastern France). Environ. Sci.
937 Technol. 51, 14038–14046.

938 Saint-André, L., M'Bou, A.T., Mabiala, A., Mouvondy, W., Jourdan, C., Roupsard, O., Deleporte, P.,
939 Hamel, O., Nouvellon, Y., 2005. Age-related equations for above- and below-ground biomass of
940 a Eucalyptus hybrid in Congo. For. Ecol. Manage. 205, 199–214.
941 https://doi.org/https://doi.org/10.1016/j.foreco.2004.10.006

942 Schlesinger, W.H., Vengosh, A., 2016. Global boron cycle in the Anthropocene. Global Biogeochem.
943 Cycles 30, 219–230. https://doi.org/10.1002/2015GB005266

944 Schmitt, A.-D., Gangloff, S., Labolle, F., Chabaux, F., Stille, P., 2017. Calcium biogeochemical cycle at
945 the beech tree-soil solution interface from the Strengbach CZO (NE France): insights from stable
946 Ca and radiogenic Sr isotopes. Geochim. Cosmochim. Acta 213, 91–109.
947 https://doi.org/https://doi.org/10.1016/j.gca.2017.06.039

948 Schuessler, J.A., von Blanckenburg, F., Bouchez, J., Uhlig, D., Hewawasam, T., 2018. Nutrient cycling in
949 a tropical montane rainforest under a supply-limited weathering regime traced by elemental
950 mass balances and Mg stable isotopes. Chem. Geol. 497, 74–87.
951 https://doi.org/https://doi.org/10.1016/j.chemgeo.2018.08.024

952 Serra, F., Guillou, C.G., Reniero, F., Ballarin, L., Cantagallo, M.I., Wieser, M., Iyer, S.S., Héberger, K.,
953 Vanhaecke, F., 2005. Determination of the geographical origin of green coffee by principal
954 component analysis of carbon, nitrogen and boron stable isotope ratios. Rapid Commun. Mass
955 Spectrom. 19, 2111–2115.

956 Shao, J.F., Yamaji, N., Huang, S., Ma, J.F., 2021. Fine regulation system for distribution of boron to
957 different tissues in rice. New Phytol. nph.17169. https://doi.org/10.1111/nph.17169

958 Shorrocks, V.M., 1997. The occurrence and correction of boron deficiency. Plant Soil 193, 121–148.

959 Spivak-Birndorf, L.J., Wang, S.-J., Bish, D.L., Wasylenki, L.E., 2018. Nickel isotope fractionation during
960 continental weathering. Chem. Geol. 476, 316–326.
961 https://doi.org/https://doi.org/10.1016/j.chemgeo.2017.11.028

962 Staelens, J., Houle, D., De Schrijver, A., Neirynck, J., Verheyen, K., 2008. Calculating dry deposition
963 and canopy exchange with the canopy budget model: review of assumptions and application to
964 two deciduous forests. Water. Air. Soil Pollut. 191, 149–169.

965 Sun, A., Xu, Q., Wei, G., Zhu, H., Chen, X., 2018. Differentiation analysis of boron isotopic
966 fractionation in different forms within plant organ samples. Phytochemistry 147, 9–13.
967 https://doi.org/https://doi.org/10.1016/j.phytochem.2017.12.012

968 Takano, J., Noguchi, K., Yasumori, M., Kobayashi, M., Gajdos, Z., Miwa, K., Hayashi, H., Yoneyama, T.,
969 Fujiwara, T., 2002. Arabidopsis boron transporter for xylem loading. Nature 420, 337–340.
970 https://doi.org/10.1038/nature01139

971 Takano, J., Tanaka, M., Toyoda, A., Miwa, K., Kasai, K., Fuji, K., Onouchi, H., Naito, S., Fujiwara, T.,
972 2010. Polar localization and degradation of Arabidopsis boron transporters through distinct
973 trafficking pathways. Proc. Natl. Acad. Sci. U. S. A. 107, 5220–5225.
974 https://doi.org/10.1073/pnas.0910744107

975 Takano, J., Wada, M., Ludewig, U., Schaaf, G., Von Wirén, N., Fujiwara, T., 2006. The Arabidopsis
976 major intrinsic protein NIP5;1 is essential for efficient boron uptake and plant development
977 under boron limitation. Plant Cell 18, 1498–1509.

978 Tanaka, M., Wallace, I.S., Takano, J., Roberts, D.M., Fujiwara, T., 2008. NIP6;1 Is a Boric Acid Channel
979 for Preferential Transport of Boron to Growing Shoot Tissues in Arabidopsis. Plant
980 Cell 20, 2860–2875. https://doi.org/10.1105/tpc.108.058628

981 Turpault, M.-P., Calvaruso, C., Kirchen, G., Redon, P.-O., Cochet, C., 2018. Contribution of fine tree
982 roots to the silicon cycle in a temperate forest ecosystem developed on three soil types.
983 Biogeosciences 15, 2231.

984 Vanderpool, R.A., Johnson, P.E., 1992. Boron isotope ratios in commercial produce and boron-10
985 foliar and hydroponic enriched plants. J. Agric. Food Chem. 40, 462–466.

986 Vogl, J., Rosner, M., Pritzkow, W., 2011. Development and validation of a single collector SF-ICPMS
987 procedure for the determination of boron isotope ratios in water and food samples. J. Anal. At.
988 Spectrom. 26, 861–869.

989 Wieser, M.E., Iyer, S.S., Krouse, H.R., Cantagallo, M.I., 2001. Variations in the boron isotope
990 composition of Coffea arabica beans. Appl. Geochemistry 16, 317–322.

991 Williams, L.B., Hervig, R.L., Holloway, J.R., Hutcheon, I., 2001. Boron isotope geochemistry during
992 diagenesis. Part I. Experimental determination of fractionation during illitization of smectite.

993 Geochim. Cosmochim. Acta 65, 1769–1782.

994 Yoshinari, A., Takano, J., 2017. Insights into the mechanisms underlying boron homeostasis in plants.
995 Front. Plant Sci. https://doi.org/10.3389/fpls.2017.01951

996

997

Fig 1: 2 columns

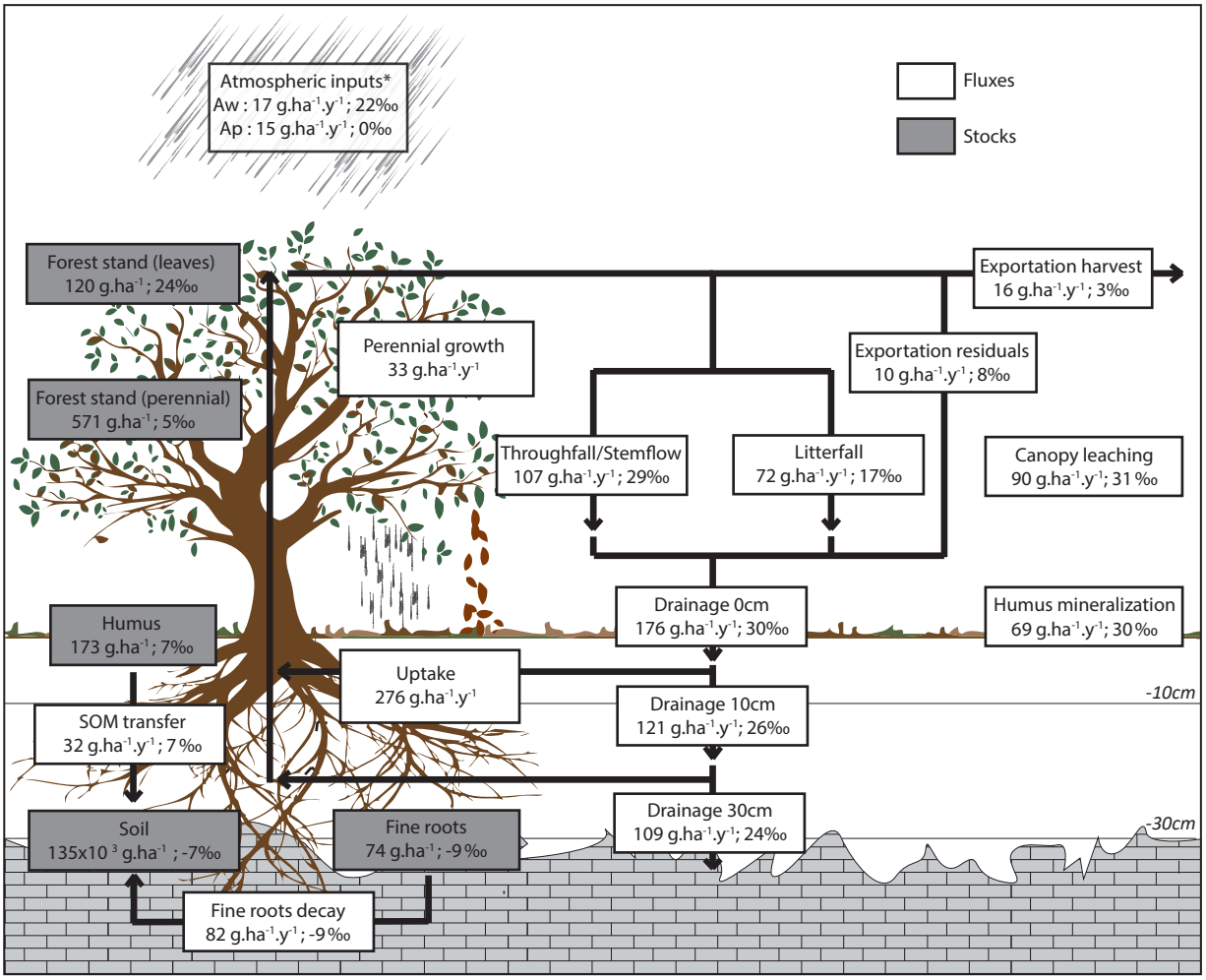

Figure 1: Biogeochemical cycle of B and B isotopes in the Montiers temperate forest ecosystem.

Fig 2: 1 column

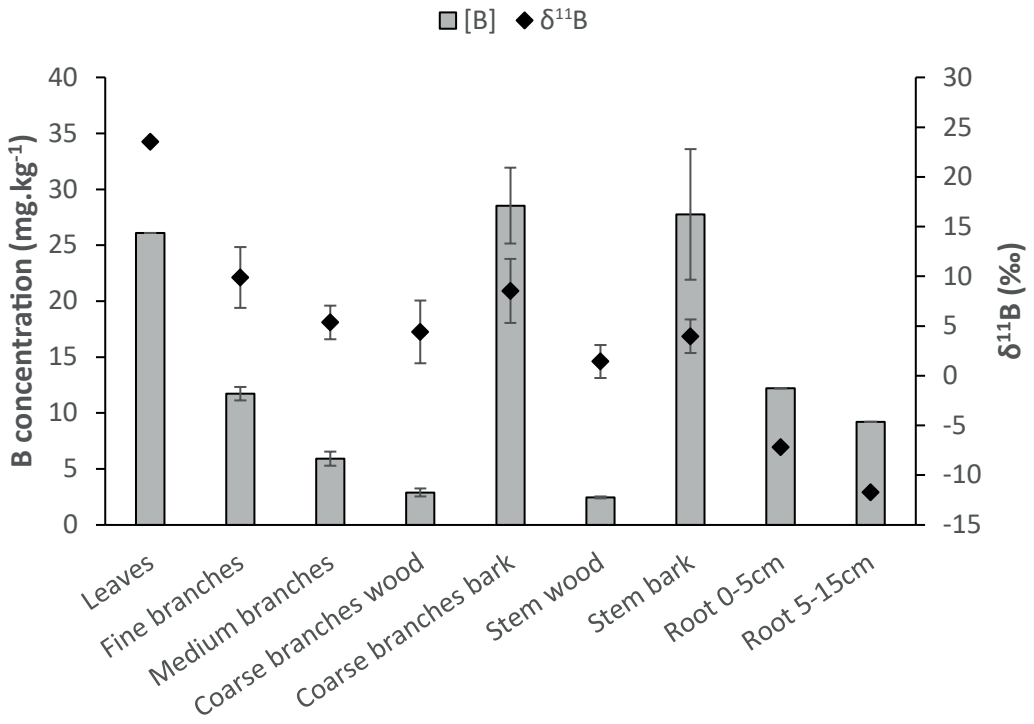

Figure 2: Boron concentration (mg.kg^{-1}) and isotopic composition (‰) of the different compartments of the beech stand.

Fig 3: 2 column

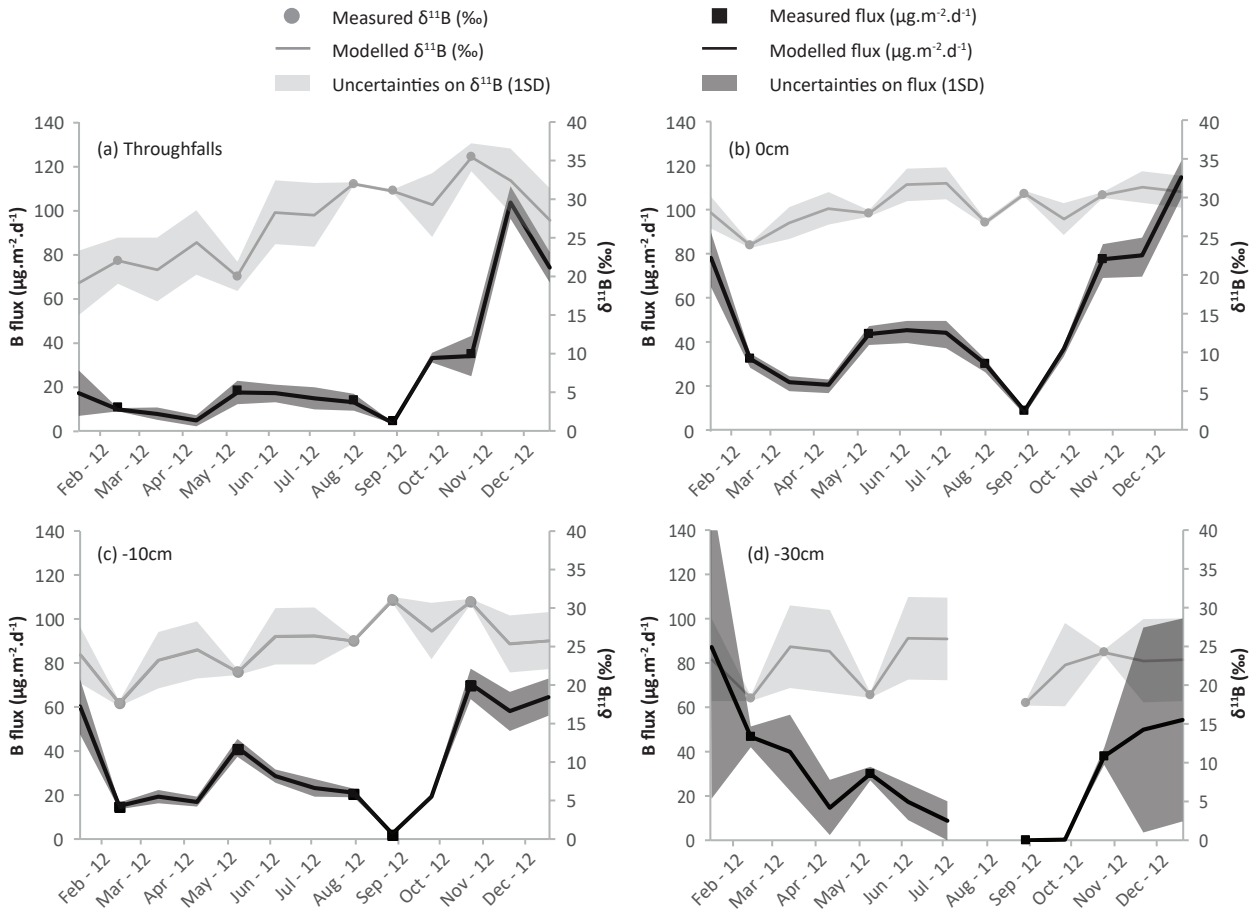

Figure 3: Modelled B fluxes (µg.m-2.d-1, in black) and isotopic compositions (‰, in grey) in (a) throughfalls, (b) soil solutions at 0 cm, (c) -10 cm and (d) -30 cm. The line corresponds to the modelled values, the dots to the measured values and the shaded area to the associated uncertainties (1SD).

Fig 4: 2 columns

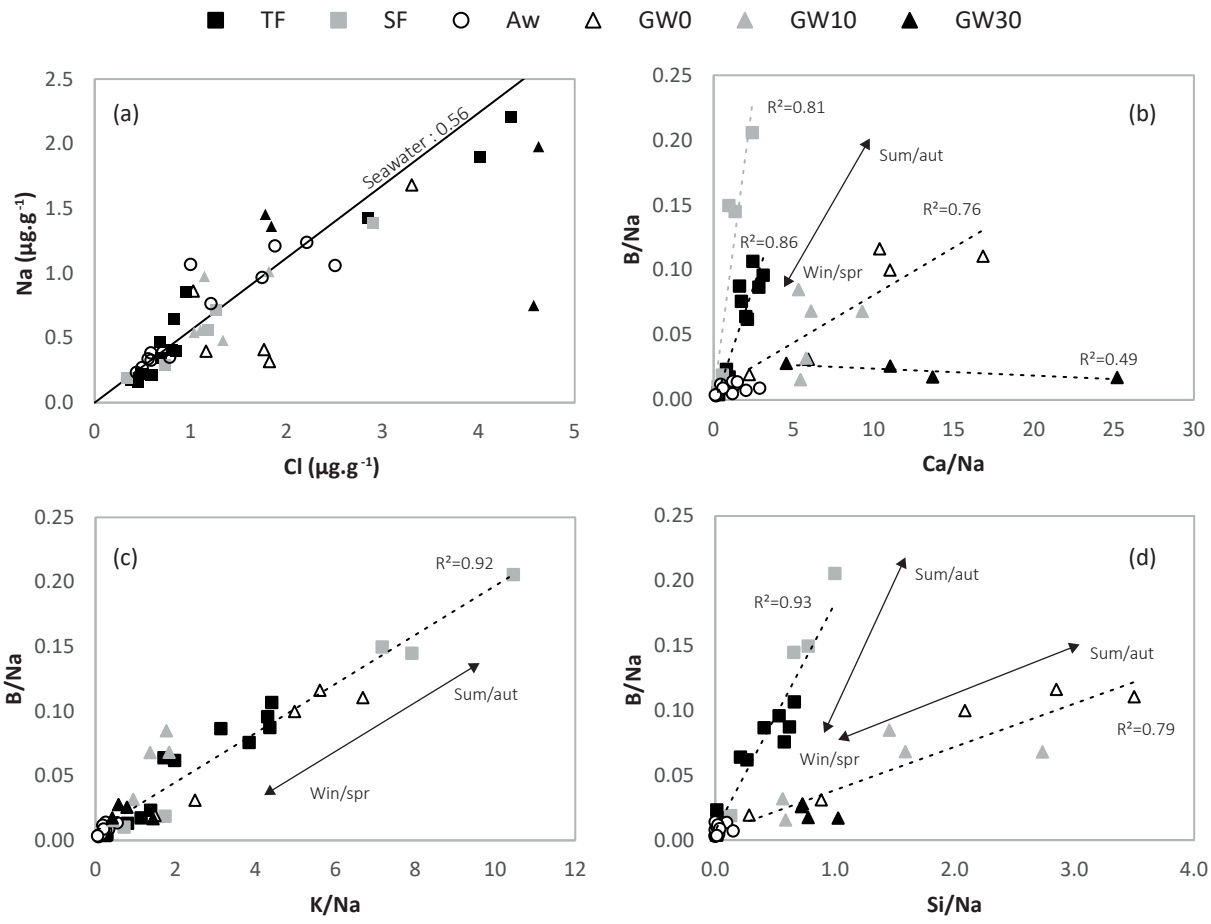

Figure 4: Comparison between (a) Na (mg.L^{-1}) and Cl (mg.L^{-1}); (b) B/Na and Ca/Na; (c) K/Na and (d) Si/Na molar ratios in all water samples collected in the Montiers forest ecosystem. TF = throughfalls; SF = stemflow; Aw = atmospheric dissolved deposition (data from Roux et al, (2017)); GW0 = soil solution at 0 cm; GW10 = soil solution at -10 cm; GW30 = soil solution at -30 cm. lines represent linear fit to help identifying similarities of differences between sub-datasets (doesn't include Aw data).

Fig 5: 1 column

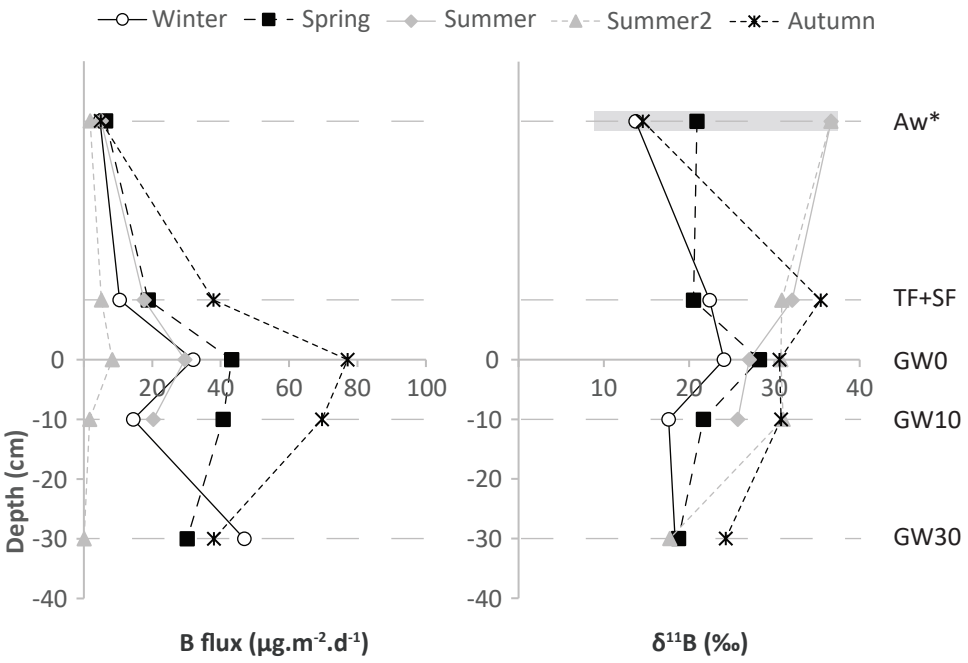

Figure 5: Seasonal variability of B fluxes and isotopic compositions evolution along the hydrological profile (from atmospheric dissolved deposition to soil solutions at -30cm). The above ground part of the hydrological profile displayed isn't to scale. Data from atmospheric dissolved deposition are from Roux et al. (2017).TF = throughfalls; SF = stemflow; Aw = Atmospheric dissolved deposition; GW0 = soil solution at 0cm; GW10 = soil solution at -10cm; GW30 = soil solution at -30cm.

Fig 6: 2 column

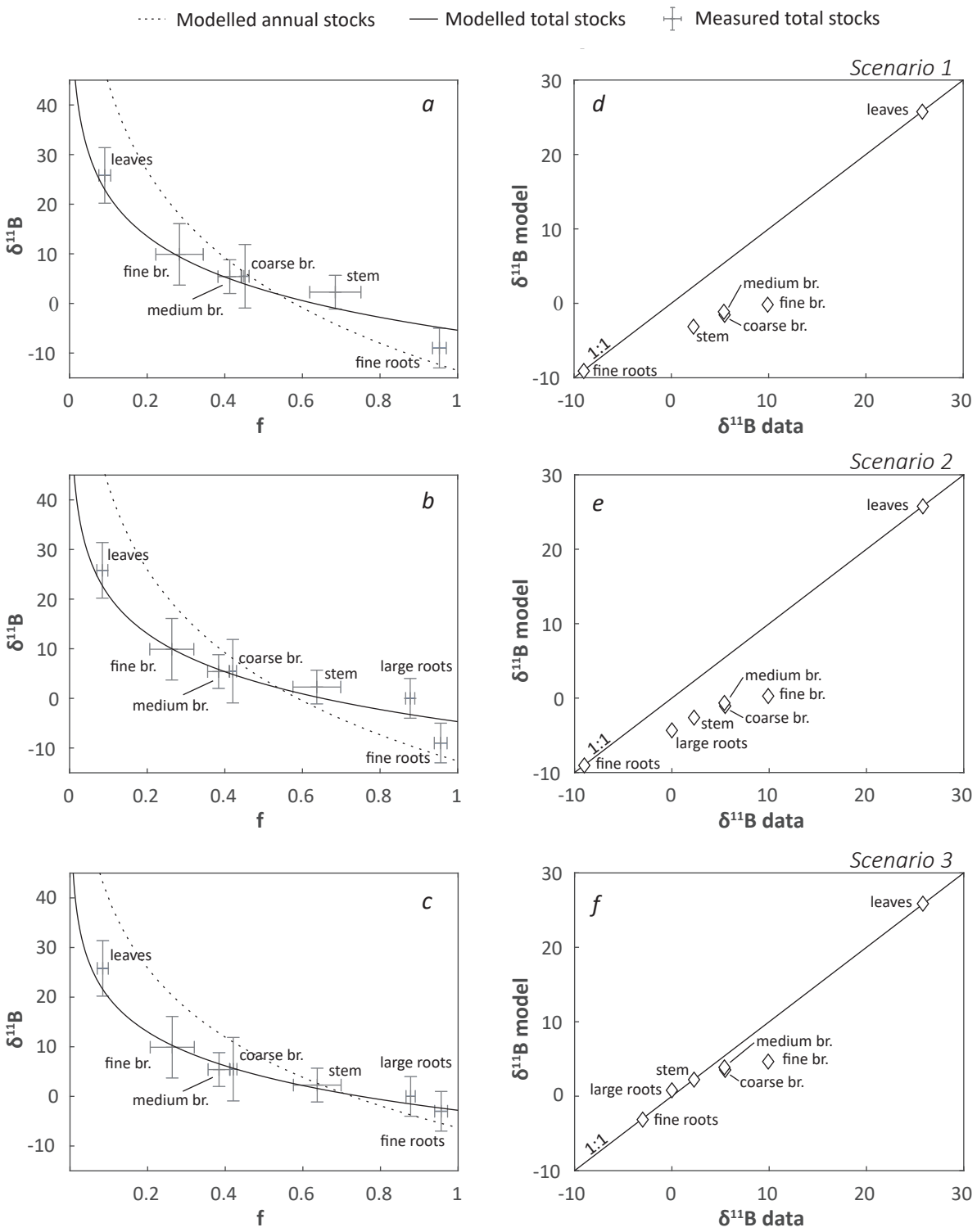

Figure 6: Results of the Rayleigh like model for B during plant growth. (a) corresponds to the annual and long-term modeling using raw data (scenario 1). (b) adds an hypothetical B stock in coarse roots based on data from Turpault et al, (2018) (scenario 2). (c) changes the $\delta^{11}B$ value of the fine root compartment to make the entire dataset consistent with Rayleigh-like behavior ($\delta^{11}B_{fine\ roots}$ = -3‰; scenario 3). (d), (e) and (f) compare the results of modelled value of annually formed biomass to the measured value in bulk intermediate organs (branches and stem) for each scenario.

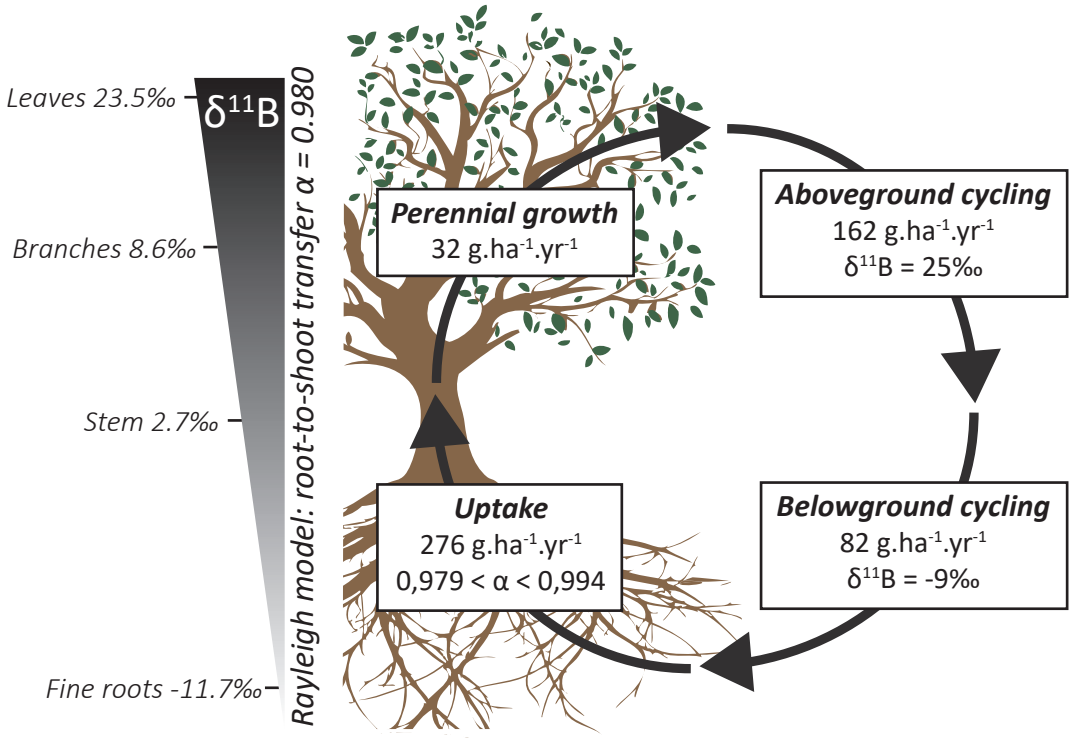
Leaves 23.5‰
δ11B
Branches 8.6‰
Stem 2.7‰
Fine roots -11.7‰
Rayleigh model: root-to-shoot transfer α = 0.980
Perennial growth
32 g.ha-1.yr-1
Aboveground cycling
162 g.ha-1.yr-1
δ11B = 25‰
Belowground cycling
82 g.ha-1.yr-1
δ11B = -9‰
Uptake
276 g.ha-1.yr-1
0,979 < α < 0,994